










# Postnatal expression of CD38 in astrocytes regulates synapse formation and adult social memory

Tsuyoshi Hattori<sup>1,\*</sup> , Stanislav M Cherepanov<sup>2</sup>, Ryo Sakaga<sup>1</sup>, Jurepon Roboon<sup>1</sup> , Dinh Thi Nguyen<sup>1</sup>, Hiroshi Ishii<sup>1</sup> , Mika Takarada-Iemata<sup>1</sup> , Takumi Nishiuchi<sup>3</sup>, Takayuki Kannon<sup>4</sup> , Kazuyoshi Hosomichi<sup>4</sup> , Atsushi Tajima<sup>4</sup> , Yasuhiko Yamamoto<sup>5</sup>, Hiroshi Okamoto<sup>5,6</sup>, Akira Sugawara<sup>7</sup> , Haruhiro Higashida<sup>2</sup> & Osamu Hori<sup>1</sup> 

## Abstract

Social behavior is essential for health, survival, and reproduction of animals; however, the role of astrocytes in social behavior remains largely unknown. The transmembrane protein CD38, which acts both as a receptor and ADP-ribosyl cyclase to produce cyclic ADP-ribose (cADPR) regulates social behaviors by promoting oxytocin release from hypothalamic neurons. CD38 is also abundantly expressed in astrocytes in the postnatal brain and is important for astroglial development. Here, we demonstrate that the astroglial-expressed CD38 plays an important role in social behavior during development. Selective deletion of CD38 in postnatal astrocytes, but not in adult astrocytes, impairs social memory without any other behavioral abnormalities. Morphological analysis shows that depletion of astroglial CD38 in the postnatal brain interferes with synapse formation in the medial prefrontal cortex (mPFC) and hippocampus. Moreover, astroglial CD38 expression promotes synaptogenesis of excitatory neurons by increasing the level of extracellular SPARCL1 (also known as Hevin), a synaptogenic protein. The release of SPARCL1 from astrocytes is regulated by CD38/cADPR/calcium signaling. These data demonstrate a novel developmental role of astrocytes in neural circuit formation and regulation of social behavior in adults.

**Keywords** astrocyte; cADPR; calcium; prefrontal cortex; social behavior

**Subject Category** Neuroscience

**DOI** 10.15252/emboj.2022111247 | Received 23 March 2022 | Revised 23 May 2023 | Accepted 31 May 2023 | Published online 26 June 2023

**The EMBO Journal (2023) 42: e111247**

## Introduction

Social behavior involves activities of, at least, two individuals of the same species, which are critical for survival, health, and reproduction (Chen & Hong, 2018). Social behavior includes spectrum of behaviors such as aggression, mating, parenting, social recognition, and social memory (Chen & Hong, 2018). To understand the regulatory mechanisms of social behaviors, the brain regions and neural circuits involved in these behaviors have been identified in rodent model systems. Among these behaviors, social memory is the ability to recall previous social interactions to make appropriate social responses (Tzakis & Holahan, 2019). Recent studies have identified critical regions for social memory such as the medial prefrontal cortex (mPFC), the hippocampal ventral CA1, and dorsal CA2 regions (Hitti & Siegelbaum, 2014; Okuyama *et al*, 2016; Oliva *et al*, 2020; Xing *et al*, 2021). Poor social function including social memory is a prominent feature of several neuropsychiatric disorders, such as autism spectrum disorder (ASD; Billeke & Aboitiz, 2013; Barak & Feng, 2016). Transgenic models of ASD display abnormal social behaviors together with abnormalities in neuronal synapses. Rett syndrome mice exhibit reduced glutamatergic synapse number, spine numbers and size of the cell bodies of neurons in the postnatal brain. They show abnormal social approach behaviors, because of their abnormal synaptogenesis of the glutamatergic neurons (Kishi & Macklis, 2004; Chao *et al*, 2007; Guy *et al*, 2007; Smrt *et al*, 2007; Samaco *et al*, 2013). Thus, proper synapse formation in the neural circuits of the developing brain is taken to be important for the establishment of social behaviors.

Astrocytes are the most abundant type of glial cells in the brain. They physically interact with neurons, provide metabolic energy

<sup>1</sup> Department of Neuroanatomy, Graduate School of Medical Sciences, Kanazawa University, Kanazawa, Japan

<sup>2</sup> Research Center for Child Mental Development, Kanazawa University, Kanazawa, Japan

<sup>3</sup> Division of Functional Genomics, Advanced Science Research Center, Kanazawa University, Kanazawa, Japan

<sup>4</sup> Department of Bioinformatics and Genomics, Graduate School of Advanced Preventive Medical Sciences, Kanazawa University, Kanazawa, Japan

<sup>5</sup> Department of Biochemistry and Molecular Vascular Biology, Graduate School of Medical Sciences, Kanazawa University, Kanazawa, Japan

<sup>6</sup> Department of Biochemistry, Tohoku University Graduate School of Medicine, Sendai, Japan

<sup>7</sup> Department of Molecular Endocrinology, Tohoku University Graduate School of Medicine, Sendai, Japan

\*Corresponding author. Tel: +81 76 265 2162; Fax: +81 76 234 4222; E-mail: thattori@staff.kanazawa-u.ac.jp

and neurotrophic factors, buffer extracellular ions, and modulate information processing and signal transmission (Lopez-Hidalgo & Schummers, 2014). Furthermore, they influence synapse formation and maintenance by releasing various molecules, contributing to the stability and plasticity of the neural circuit (Chung *et al*, 2015; Augusto-Oliveira *et al*, 2020). Through interaction between astrocytes and neurons, astrocytes have been shown to affect cognitive processing, including learning, memory, and attention, by regulating the synaptic connectivity of neural networks (Orr *et al*, 2015; Nagai *et al*, 2019). Interestingly, a previous study showed that mice engrafted with human astrocytes exhibited improved learning as well as enhanced long-term potentiation in the hippocampus (Han *et al*, 2013). These studies indicate that astrocytes play important roles in neuronal circuit formation and cognitive behavior; however, the involvement of astrocytes in social behavior is largely unknown.

CD38 is a multifunctional transmembrane protein that possesses ADP-ribosyl cyclase activity, which produces cyclic ADP-ribose (cADPR) from nicotinamide adenine dinucleotide (NAD<sup>+</sup>) and releases Ca<sup>2+</sup> from intracellular stores (Lee, 2001; Guse, 2005; Malavasi *et al*, 2008; Okamoto & Takasawa, 2021). CD38 has been shown to promote the secretion of oxytocin from hypothalamic neurons by elevating intracellular calcium concentration, affecting social behaviors such as social recognition and rearing behavior (Jin *et al*, 2007). CD38 is predominantly expressed in astrocytes in the cortex, and astroglial CD38 promotes the maturation of astrocytes cell-autonomously and differentiation of oligodendrocytes non-cell-autonomously (Hattori *et al*, 2017). These studies suggest that astroglial CD38 plays a pivotal role in brain development through gli-glia crosstalk. However, the roles of astroglial CD38 in neural circuit formation and social behavior remains unknown.

In this study, we assessed the role of astroglial CD38 in social behavior and neuronal development. Selective deletion of astrocytic CD38 in the postnatal brain specifically impaired social memory and reduced excitatory synapse formation in the medial prefrontal cortex (mPFC) and hippocampus. Astroglial CD38 promoted excitatory synapse formation through SPARCL1 (also known as Hevin), a synaptogenesis-promoting protein in the postnatal brain. Finally, SPARCL1 secretion was regulated by CD38/cADPR/calcium signaling in astrocytes.

## Results

### Deletion of astroglial CD38 in postnatal brain impairs social memory

We previously showed that CD38 expression peaked from postnatal day 14 (P14) to P28 in the cortex and was most abundantly expressed in astrocytes during that period (Hattori *et al*, 2017). To investigate the role of astroglial CD38 in social behavior, we generated conditional knockout mice in which *Cd38* gene was selectively deleted in astrocytes of the postnatal brain using *CreERT2-LoxP* recombination technology. As GLAST-CreER<sup>T2</sup>-mediated recombination has been widely used to express transgenes and delete genes in astrocyte *in vivo* (Bardehle *et al*, 2013; Barca-Mayo *et al*, 2017; Zhang *et al*, 2020), homozygous *Cd38<sup>flox/flox</sup>* mice were crossed with *Glast<sup>CreERT2/+</sup>* mice to generate *Cd38<sup>flox/flox</sup>;Glast<sup>CreERT2/+</sup>* mice. Tamoxifen was injected to *Cd38<sup>flox/flox</sup>;Glast<sup>+/+</sup>* or *Cd38<sup>flox/flox</sup>*;

*Glast<sup>CreERT2/+</sup>* mice once a day for five consecutive days at P10–P14 (ctrl<sup>P10</sup> or CD38 AS-cKO<sup>P10</sup>, respectively; Fig 1A). To confirm astrocyte-specific deletion of CD38, we isolated astrocytes from the medial prefrontal cortex (mPFC) and hippocampus of ctrl<sup>P10</sup> and CD38 AS-cKO<sup>P10</sup> mice at P20 by magnetic-activated cell sorting (MACS) using the astrocyte surface antigen ACSA2 as previously described (Kantzer *et al*, 2017; Holt *et al*, 2019; Ohlig *et al*, 2021), and then we examined *Cd38* mRNA expression. We confirmed enrichment of astrocytes and other types of cells such as neurons, microglia and oligodendrocyte progenitor cells in the ACSA2 positive and negative fractions, respectively, by measuring *S100b* and *Slc17a7* (VGlut1), *Iba1* and *Pdgfra* mRNA levels (Fig EV1B–E and G–J). *Cd38* mRNA was substantially decreased in the astrocyte-enriched fraction, while, *Cd38* expression was not changed in ACSA2 negative fractions in the mPFC and hippocampus (Fig EV1A and F). Further western blot analysis demonstrated that CD38 expression in the mPFC was significantly reduced in CD38 AS-cKO<sup>P10</sup> mice compared to ctrl<sup>P10</sup> littermates at P21, indicating predominant expression of CD38 in astrocytes (Fig EV2A and B).

Next, we investigated astroglial development in these CD38 AS-cKO<sup>P10</sup> mice. Consistent with our previous study using constitutive CD38 KO mice (Hattori *et al*, 2017), the expression of astrocyte-specific molecules, GFAP and Cx43 were significantly decreased in the mPFC of CD38 AS-cKO<sup>P10</sup> mice at P21 (Fig EV2A, C, and D). On the other hand, the expression of NDRG2, another astrocyte-specific protein was not changed in these mice (Fig EV2A and E). Immunohistochemical analysis also showed that the number of GFAP and S100β positive astrocytes decreased in the mPFC of CD38 AS-cKO<sup>P10</sup> mice at P21 (Fig EV2K–N). However, the number of NDRG2 and SOX9 positive astrocytes did not change in these mice (Fig EV2O–R). These results suggest the altered expression of several astrocyte-specific proteins without changing the total number of astrocytes in CD38 AS-cKO<sup>P10</sup> mice. Further analysis revealed that unlike decreased myelination in constitutive CD38 KO mice (Hattori *et al*, 2017), MAG and MBP expression, myelin proteins, were not altered in the cerebral cortex of CD38 AS-cKO<sup>P10</sup> mice (Fig EV2A, H, S and T). These results indicate that astrocyte-specific deletion of CD38 at P10 impairs the postnatal development of astrocytes without affecting myelination.

Multiple studies have reported that constitutive CD38 KO mice exhibit impaired social behaviors (Kim *et al*, 2016; Martucci *et al*, 2019; Gerasimenko *et al*, 2020). To investigate whether astrocytic CD38 is involved in social behavior, we conducted a three-chamber social approach test on CD38 AS-cKO<sup>P10</sup> mice (Fig 1B). In the first phase, test mice were allowed to freely explore an object and stranger 1 (sociability). Both ctrl<sup>P10</sup> and CD38 AS-cKO<sup>P10</sup> mice showed a significant preference for exploring stranger 1 (Fig 1C). Immediately after the sociability test, the test mice were allowed to freely explore novel stranger 2 and the now-familiar stranger 1 (social preference). Both ctrl<sup>P10</sup> and CD38 AS-cKO<sup>P10</sup> mice demonstrated similar preference for social novelty (Fig 1D). After a 30-min interval, we performed the test again, with novel stranger 3 replaced from the stranger 2 (social memory). Control mice spent more time investigating novel stranger 3 than the familiar stranger 1, whereas CD38 AS-cKO<sup>P10</sup> mice showed similar investigation times between the familiar and stranger mouse (Fig 1E). These results indicate that CD38 AS-cKO<sup>P10</sup> mice have no deficit in sociability and social preference, but a clear deficit in social memory. To compare social

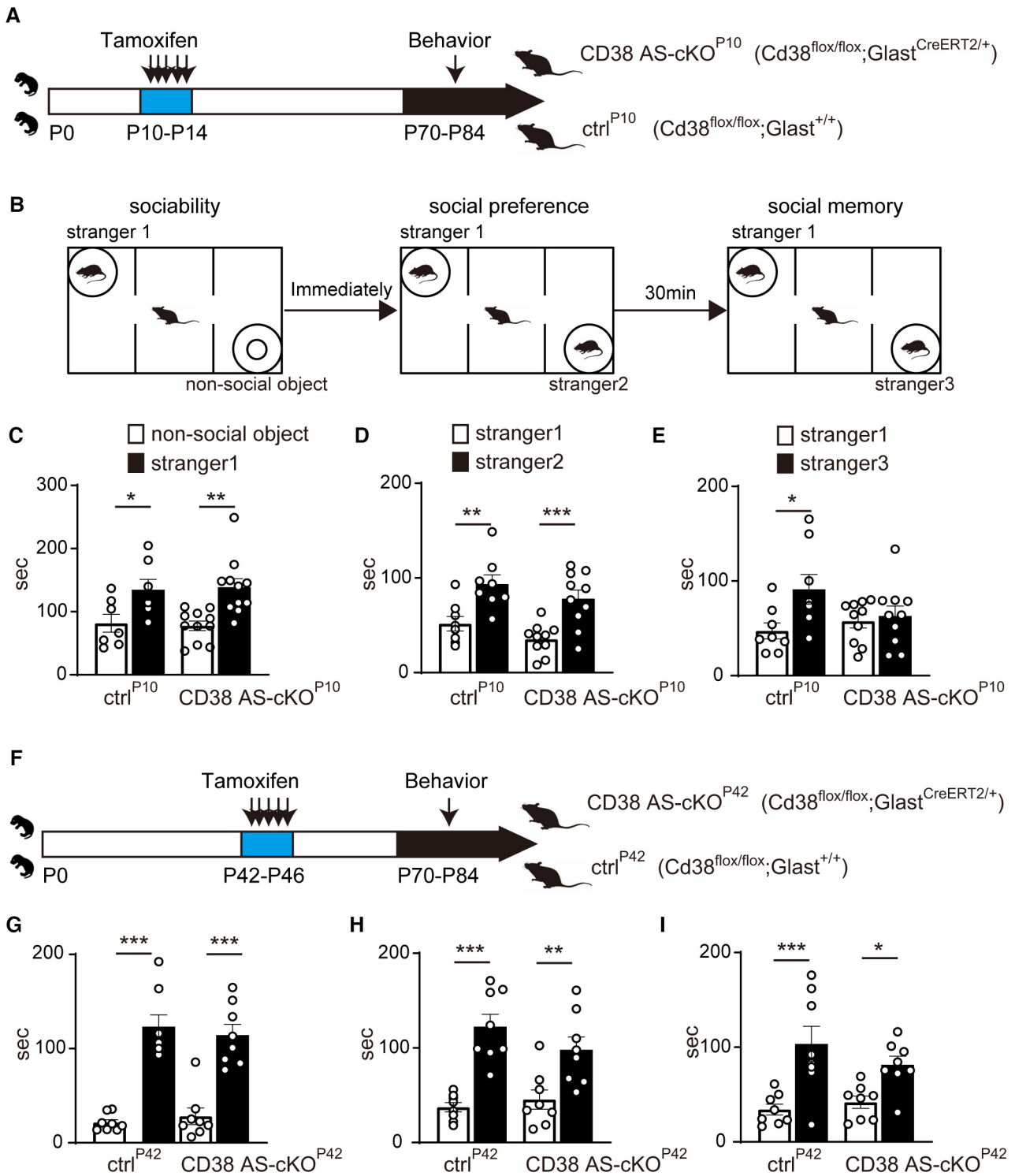


**Figure 1. Deletion of astroglial CD38 in postnatal brain impairs social memory.**

A–I (A, F) Paradigm for inducing astrocyte-specific deletion of CD38 from P10 in ctrl<sup>P10</sup> and CD38 AS-cKO<sup>P10</sup> mice (A) or from P42 in ctrl<sup>P42</sup> and CD38 AS-cKO<sup>P42</sup> mice (F) and behavior tests. (B) Schematic diagram of social behavior tests in the three chamber test. (C, G) Sociability of ctrl<sup>P10</sup> and CD38 AS-cKO<sup>P10</sup> mice (C) or ctrl<sup>P42</sup> and CD38 AS-cKO<sup>P42</sup> (G) mice ( $n = 7–10$  animals per genotype). (D, H) Social novelty of ctrl<sup>P10</sup> and CD38 AS-cKO<sup>P10</sup> mice (D) or ctrl<sup>P42</sup> and CD38 AS-cKO<sup>P42</sup> (H) mice ( $n = 7–10$  animals per genotype). (E, I) Social memory of ctrl<sup>P10</sup> and CD38 AS-cKO<sup>P10</sup> mice (E) or ctrl<sup>P42</sup> and CD38 AS-cKO<sup>P42</sup> (I) mice ( $n = 7–10$  animals per genotype).

Data information: Data represent means  $\pm$  SEM. \* $P < 0.05$ , \*\* $P < 0.01$ , \*\*\* $P < 0.001$  (two-way ANOVA followed by Bonferroni's multiple comparisons test).

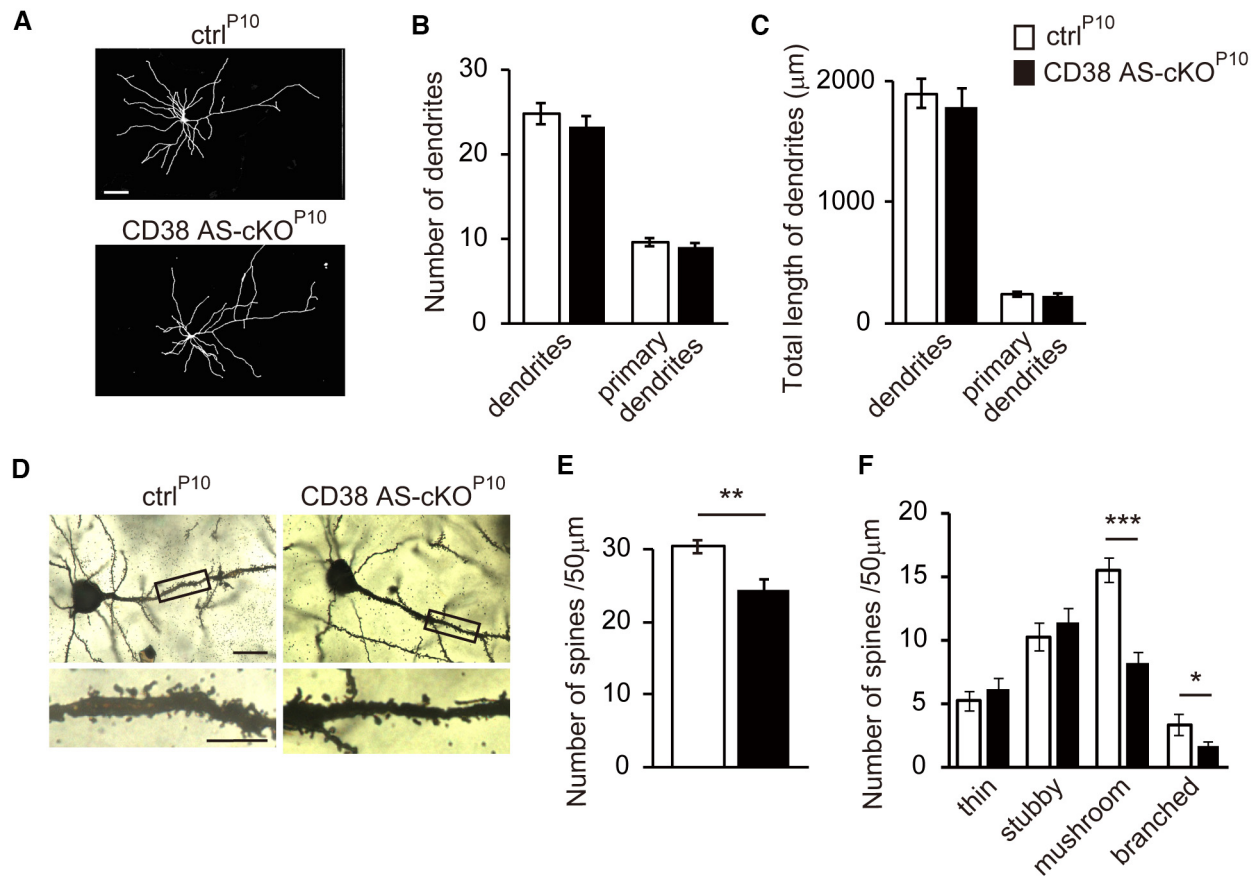


**Figure 2. Spine morphology is altered in the mPFC pyramidal neurons in CD38 AS-cKO<sup>P10</sup> mice.**

A Images of tracing of Golgi-stained pyramidal neurons in the mPFC of ctrl<sup>P10</sup> and CD38 AS-cKO<sup>P10</sup> mice at P70. Scale bar, 20 μm.  
 B, C Quantification of the total number (B) or total length (C) of dendrites and primary dendrites in ctrl<sup>P10</sup> and CD38 AS-cKO<sup>P10</sup> mice ( $n = 24$  cells from four animals per genotype, two-way ANOVA followed by Bonferroni's multiple comparisons test).  
 D Images of Golgi-stained pyramidal neurons in the mPFC of ctrl<sup>P10</sup> and CD38 AS-cKO<sup>P10</sup> mice at P70. Scale bars, 20 μm (upper) and 5 μm (lower).  
 E Quantification of the total number of spines on the apical dendrites of the ctrl<sup>P10</sup> and CD38 AS-cKO<sup>P10</sup> mice ( $n = 24$  dendrites from four animals per genotype, two-tailed unpaired Student's *t*-test).  
 F The percentage of branched, mushroom, stubby, and thin spines in cortical apical dendritic spines of the ctrl<sup>P10</sup> and CD38 AS-cKO<sup>P10</sup> mice ( $n = 24$  dendrites from four animals per genotype, two-way ANOVA followed by Bonferroni's multiple comparisons test).

Data information: Data represent means ± SEM. \* $P < 0.05$ , \*\* $P < 0.01$ , \*\*\* $P < 0.001$ .

behaviors between constitutive CD38 KO and CD38 AS-cKO<sup>P10</sup> mice, we further performed three chamber test of constitutive CD38 KO mice. Unlike CD38 AS-cKO<sup>P10</sup> mice, constitutive CD38 KO mice showed abnormalities in both social memory and social preference (Fig EV3A–C). Next, to investigate whether the deficit in CD38 AS-cKO<sup>P10</sup> mice is attributed to abnormal brain development, we performed social behavior tests on *Cd38<sup>f/f</sup>;Glast<sup>+/+</sup>* or *Cd38<sup>f/f</sup>;Glast<sup>CreERT2/+</sup>* mice in which tamoxifen was injected from P42 to P46 (ctrl<sup>P42</sup> or CD38 AS-cKO<sup>P42</sup>, respectively; Fig 1F). We confirmed significant reduction of CD38 protein expression in the mPFC of CD38 AS-cKO<sup>P42</sup> mice (Fig EV2I and J). In these mice, all social behaviors, sociability, social preference, and social memory were similar to those of ctrl<sup>P42</sup> mice (Fig 1G–I and Dataset EV4). Furthermore, constitutive CD38 KO mice have been reported to exhibit impaired parental, depression-like and hedonic behavior due to decreased plasma oxytocin levels (Cherepanov *et al*, 2017). Thus, we performed a parental retrieval test, tail suspension test, sucrose

preference test, elevated plus maze test, object recognition test and odor discrimination test. However, CD38 AS-cKO<sup>P10</sup> mice did not show any significant differences in these behavioral tests (Fig EV4A–I) or in plasma oxytocin levels compared to ctrl<sup>P10</sup> mice (Fig EV4J). These results indicate that the deletion of astroglial CD38 specifically causes social memory deficits by disturbing postnatal brain development.

#### Deletion of astroglial CD38 in postnatal brain impairs synapse formation

Previous studies have shown that the mPFC, ventral CA1, and dorsal CA2 regions of the hippocampus are essential for social memory (Okuyama *et al*, 2016; Oliva *et al*, 2020; Sun *et al*, 2020). Furthermore, CD38 KO mice display prefrontal cortex dysfunction, such as impaired synaptic plasticity and excitation–inhibition balance (Martucci *et al*, 2019). Thus, we investigated neuronal development



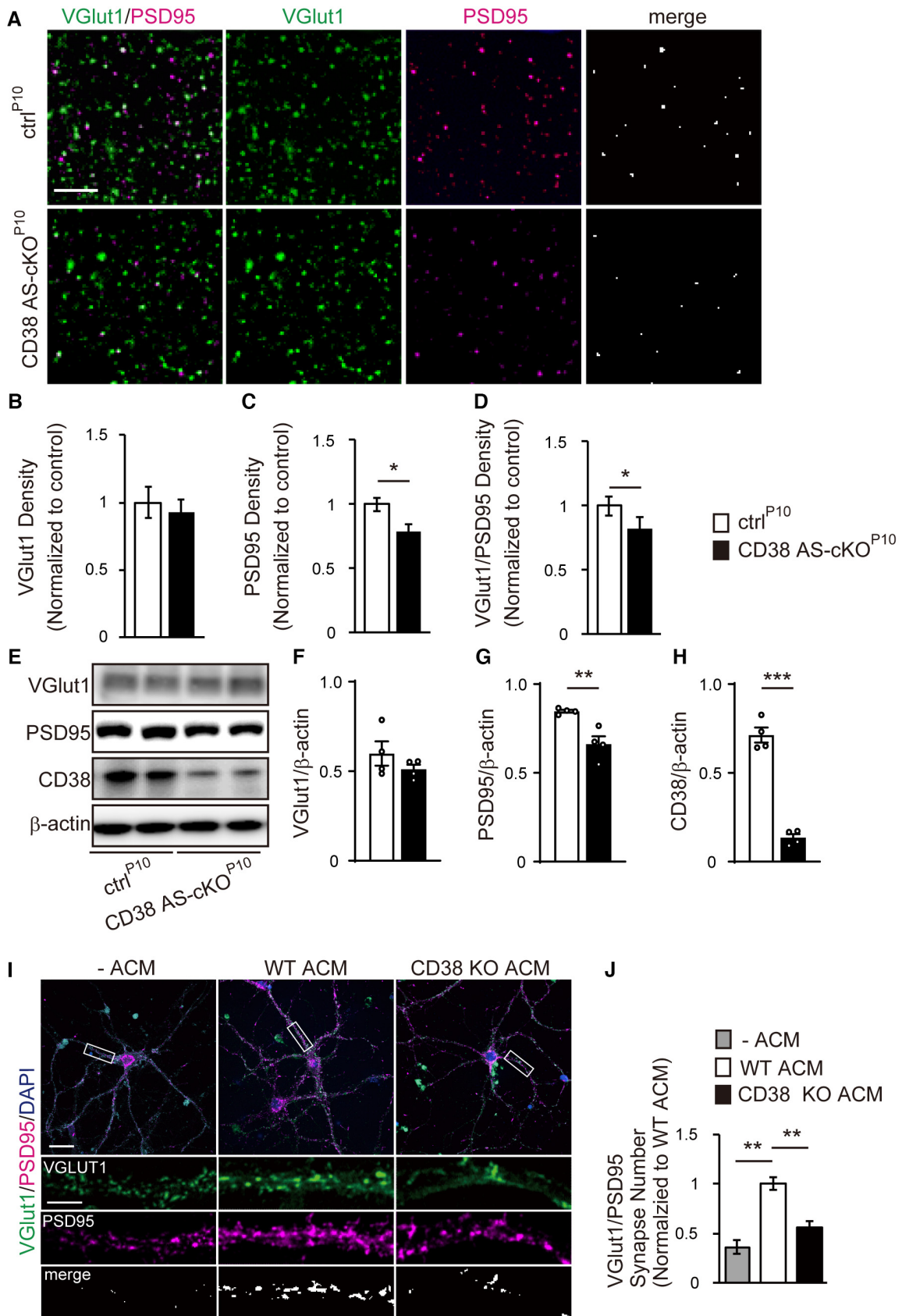


Figure 3.

**Figure 3. Astroglial CD38 promotes synapse formation of cortical neurons in the mPFC.**

- A Immunohistochemistry for VGlut1 (green) and PSD95 (magenta) in the mPFC of ctrl<sup>P10</sup> and CD38 AS-cKO<sup>P10</sup> mice at P70. VGlut1 and PSD95 channels are separated in the middle panels. The right panels are colocalized VGlut1 and PSD95 puncta (synapses). Scale bar, 10  $\mu$ m.
- B–D Quantification of VGlut1, PSD95 and synapse density in the mPFC of CD38 AS-cKO<sup>P10</sup> and ctrl<sup>P10</sup> mice ( $n = 5$  animals per genotype, two-tailed unpaired Student's *t*-test (B, C), Mann–Whitney *U*-test (D)).
- E Representative western blots of VGlut1, PSD95, CD38, and  $\beta$ -actin in the mPFC of ctrl<sup>P10</sup> and CD38 AS-cKO<sup>P10</sup> mice at P70 (two animals per genotype are shown).
- F–H Relative optical density of VGlut1, PSD95, and CD38 normalized to that of the loading control  $\beta$ -actin ( $n = 4$  animals per genotype, two-tailed unpaired Student's *t*-test).
- I Representative images of cortical neurons cultured for 14 days *in vitro* (DIV) in non-conditioned growth medium (–ACM) or astrocyte conditioned medium (ACM) of WT or CD38 KO mice. Insets show individual channels for VGlut1 (green) and PSD95 (magenta) staining, as well as the merged image. Nuclei were counterstained with DAPI. Scale bar, 20  $\mu$ m (main image) and 10  $\mu$ m (inset).
- J Quantification of synapse number in cortical neurons cultured in –ACM, WT ACM and CD38 KO ACM ( $n = 20$  cells per condition from four independent cultures, one-way ANOVA followed by Tukey–Kramer test).
- Data information: Data represent means  $\pm$  SEM. \* $P < 0.05$ , \*\* $P < 0.01$ , \*\*\* $P < 0.001$ . Source data are available online for this figure.

in the mPFC of CD38 AS-cKO<sup>P10</sup> mice. Golgi staining was performed to reveal changes in the dendrites, spine density, and spine morphology in CD38 AS-cKO<sup>P10</sup> mice at P70. The Number and total length of all dendrites and primary dendrites were quantified in cortical pyramidal neurons of the mPFC. Consistent with a previous study on the motor and somatosensory cortex of constitutive CD38 KO mice (Nelissen *et al*, 2018), the indices of dendrites in CD38 AS-cKO<sup>P10</sup> were not different from those of ctrl<sup>P10</sup> mice (Fig 2A–C). Next, spine density and morphology were analyzed in the apical dendrites of cortical pyramidal neurons in the mPFC of CD38 AS-cKO<sup>P10</sup> mice. Spine morphology was categorized into four groups, mushroom, branched, thin, and stubby spines. Mushroom and branched spines represent mature spines that have larger, more complex postsynaptic density, and are functionally stronger in response to glutamate. Thin spines and stubby spines represent immature spines that are flexible, rapidly enlarging or shrinking in brain development. Total spine densities were significantly reduced in apical dendrite of CD38 AS-cKO<sup>P10</sup> mice (Fig 2D and E). Among the four spine types, mushroom and branched spines were significantly decreased in CD38 AS-cKO<sup>P10</sup> mice. On the other hand, the number of thin and stubby spines did not change in CD38 AS-cKO<sup>P10</sup> mice (Fig 2D and F). We further performed a morphological analysis of the cortical neurons in the mPFC of constitutive CD38 KO mice. Consistent with CD38 AS-cKO<sup>P10</sup> mice, constitutive CD38 KO mice showed decreased total spine and mature spine numbers (Appendix Fig S1D–F). However, in contrast to CD38 AS-cKO<sup>P10</sup> mice, constitutive CD38 KO mice showed a slight decrease in primary dendrites (Appendix Fig S1A–C).

Next, we assessed whether the number of synapses was decreased in the mPFC of CD38 AS-cKO<sup>P10</sup> mice at P70 by immunostaining of pre- and postsynaptic proteins, vesicular glutamate transporter 1 (VGlut1), and postsynaptic density protein 95 (PSD95). While there was no significant change in the density of VGlut1 immunoreactivity in CD38 AS-cKO<sup>P10</sup> mice compared to that in littermate ctrl<sup>P10</sup> mice, there was a significant decrease in the density of PSD95 in CD38 AS-cKO<sup>P10</sup> mice (Fig 3A–C). Consistent with the reduction in spine numbers and PSD95 expression, there was a significant decrease in the number of synapses defined as colocalized presynaptic VGlut1 and postsynaptic PSD95 immunoreactivity in CD38 AS-cKO<sup>P10</sup> mice (Fig 3A and D). On the other hand, the number of synapses colocalized with VGlut2, another presynaptic protein, and PSD95 was not changed in the mPFC of CD38 AS-cKO<sup>P10</sup> mice (Appendix Fig S2A and B). Western blotting analysis also

revealed significantly decreased CD38 and PSD95 expression in CD38 AS-cKO<sup>P10</sup> mice at P70 and P21 (Figs 3E–H, and EV2A, B, F and G). We further investigated synapse numbers in other social memory-related regions, such as hippocampal CA1 and CA2 of CD38 AS-cKO<sup>P10</sup> mice at P70 (Hitti & Siegelbaum, 2014; Okuyama *et al*, 2016). The number of synapses was significantly decreased in the stratum radiatum of the CD38 AS-cKO<sup>P10</sup> CA1 and CA2 regions (Fig EV5A–D). Next, we examined the number of synapses in the mPFC of CD38 AS-cKO<sup>P42</sup> mice, which did not exhibit social memory impairment. VGlut1, PSD95 or synapse density was not altered in CD38 AS-cKO<sup>P42</sup> mice (Appendix Fig S3A and B), indicating that astroglial CD38 developmentally regulates synapse formation. Finally, constitutive CD38 KO mice showed similarly decreased synapse numbers in the mPFC (Appendix Fig S4A–D and Dataset EV4), suggesting that CD38 in other types of cells does not contribute much to synaptogenesis. Taken together, these results indicate that astroglial CD38 developmentally regulates excitatory synapse formation in the mPFC and the CA1 and CA2 of the hippocampus.

**Astroglial CD38 promotes synapse formation of cortical neurons through secreted molecules**

Astrocyte-conditioned medium (ACM) has a profound enhancement effect on synapse formation in neurons (Chung *et al*, 2015). To determine whether astroglial CD38 affects synaptic formation through secreted molecules, primary cortical neurons were cultured in non-conditioned culture medium, WT- or CD38 KO-ACM from 4 to 14 days *in vitro* (DIV). The synaptic density was evaluated by immunostaining with anti-VGlut1 and -PSD95 antibodies. The number of synapses defined as colocalization of VGlut1 and PSD95 was significantly increased by WT ACM compared with non-conditioned growth medium (Fig 3I and J). While, the number of synapses was significantly lower in neurons with CD38 KO-ACM than in those in WT-ACM (Fig 3I and J). On the other hand, there was no difference in the length of dendrites or viability between neurons cultured with WT- and CD38 KO-ACM (Appendix Fig S5A–E). These results indicate that deletion of astroglial CD38 suppresses synapse formation through extracellular molecules.

**Astroglial CD38 promotes synapse formation through SPARCL1**

To identify the extracellular molecules responsible for the decreased synapses in the mPFC of CD38 AS-cKO<sup>P10</sup> mice and primary neurons

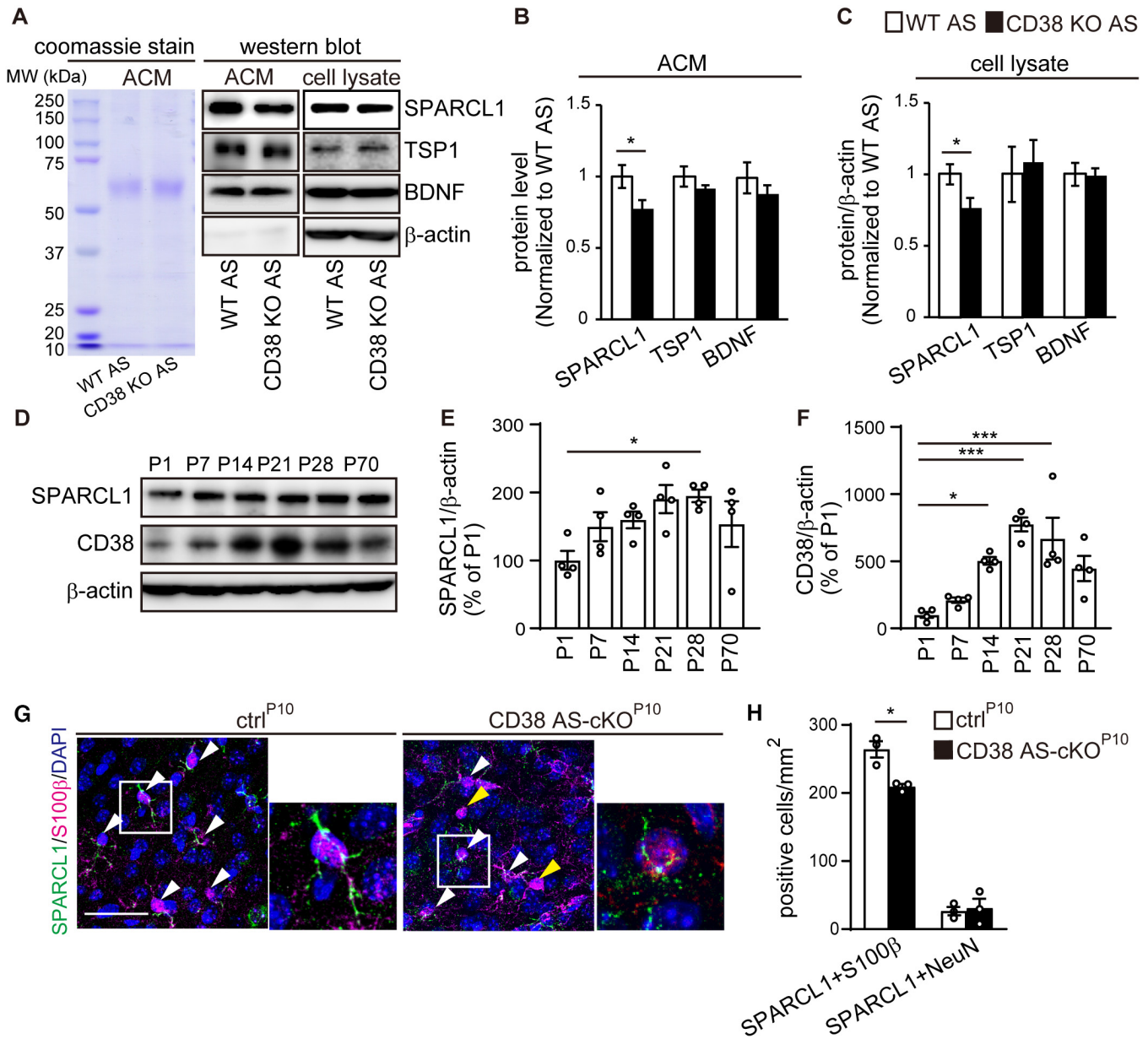


**Figure 4. Astroglial CD38 regulates extracellular SPARCL1 level.**

A Coomassie staining shows the total protein composition of ACM of WT and CD38 KO astrocytes. Representative western blot images of SPARCL1, TSP1, BDNF, and  $\beta$ -actin protein expression in ACM and cell lysates derived from WT or CD38 KO astrocytes.

B, C SPARCL1, TSP1, and BDNF level in ACM and cell lysates derived from WT or CD38 KO astrocytes. Protein levels in ACM and lysates were normalized to total protein and the loading control  $\beta$ -actin, respectively ( $n = 6$  independent culture per condition from six animals, two-tailed unpaired Student's  $t$ -test).

D Representative western blot images of SPARCL1, CD38, and  $\beta$ -actin protein expression in the postnatal mPFC of WT mice.

E, F Relative optical density of SPARCL1 and CD38 normalized to that of the loading control  $\beta$ -actin ( $n = 4$  animals, one-way ANOVA followed by Tukey–Kramer test).

G Immunohistochemistry for SPARCL1 (green) and S100 $\beta$  (magenta) in the mPFC of ctrl<sup>P10</sup> and CD38 AS-cKO<sup>P10</sup> mice at P21. White arrowheads indicate SPARCL1/S100 $\beta$ -double positive cells. Yellow arrowheads indicate SPARCL1-negative/S100 $\beta$ -positive cells. Nuclei were counterstained with DAPI. Scale bar, 50  $\mu$ m.

H Quantification of SPARCL1/S100 $\beta$ - or SPARCL1/NeuN-double positive cells in the mPFC of ctrl<sup>P10</sup> and CD38 AS-cKO<sup>P10</sup> mice at P21 ( $n = 3$  animals per genotype, two-tailed unpaired Student's  $t$ -test).

Data information: Data represent means  $\pm$  SEM. \* $P < 0.05$ , \*\*\* $P < 0.001$ . Source data are available online for this figure.

treated with CD38 KO-ACM, we performed proteomic analysis of WT- and CD38 KO-ACM. A total of 118 proteins were identified by LC-MS/MS analysis of WT-ACM and CD38 KO-ACM (Dataset EV1). Proteins

with an abundance ratio of (CD38 KO ACM)/(WT ACM) of  $1.5 >$  or  $< 0.67$  and abundance ratio variability (%)  $< 15$  were subjected to gene ontology (GO) analysis. Five extracellular proteins



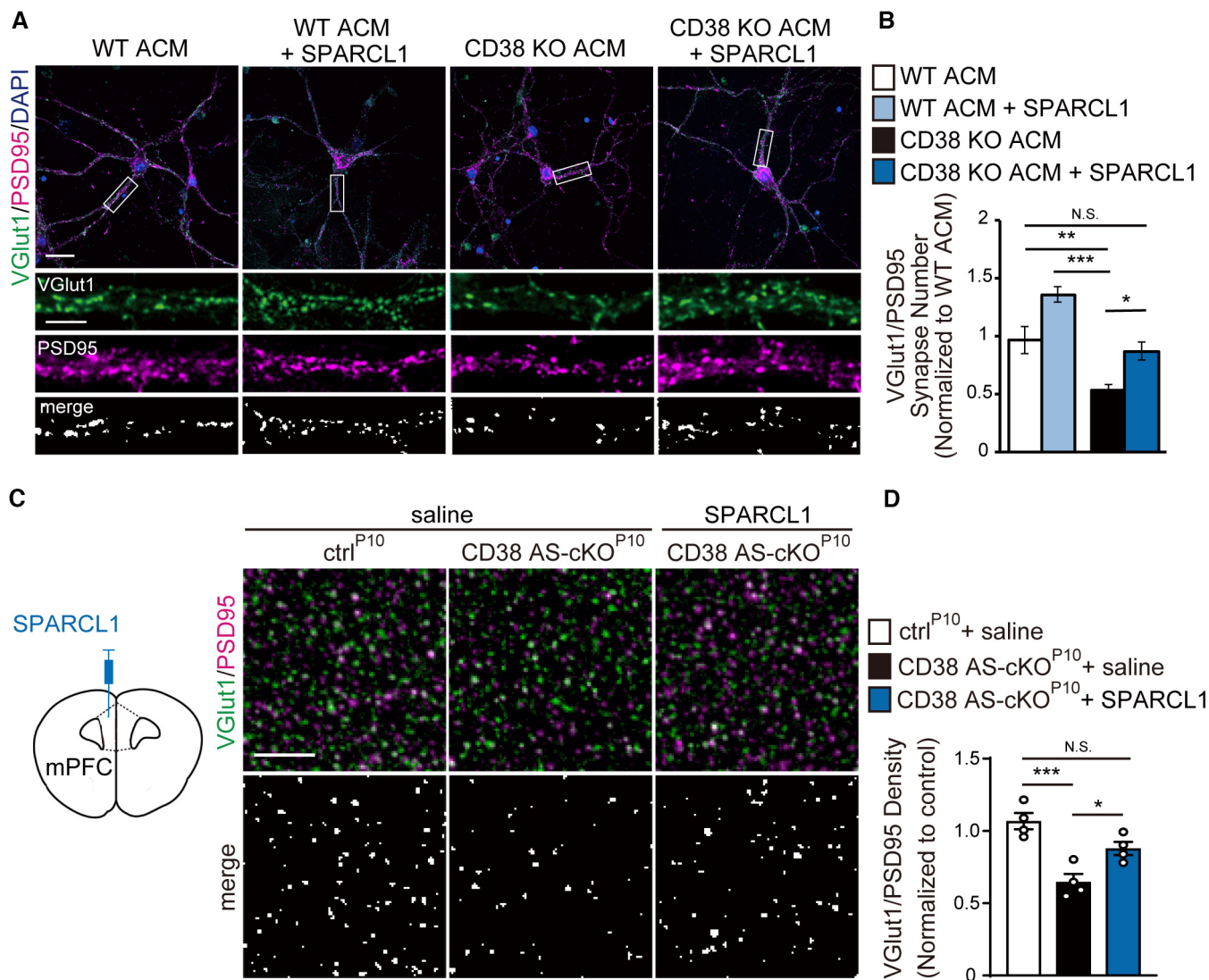


**Figure 5. Astroglial CD38 promotes synapse formation through SPARCL1.**

**A** Representative images of cortical neurons cultured for 14 DIV in WT ACM, WT ACM with SPARCL1, CD38 KO ACM, and CD38 KO ACM with SPARCL1 proteins. The insets show individual channels for VGlut1 (green) and PSD95 (magenta) staining, as well as the merged image. Nuclei were counterstained with DAPI. Scale bars: 20  $\mu$ m (main image) and 10  $\mu$ m (inset).

**B** Quantification of synapse numbers in cortical neurons ( $n = 40$  to 55 cells per condition from five independent cultures, one-way ANOVA followed by Tukey–Kramer test).

**C** SPARCL1 protein was stereotactically injected directly into layer II/III of the CD38 AS-cKO<sup>P10</sup> mPFC at P15. Immunohistochemistry for VGlut1 (green) and PSD95 (magenta) in the mPFC of ctrl<sup>P10</sup> and CD38 AS-cKO<sup>P10</sup> mice at P18. The lower panels show the colocalized VGlut1 and PSD95 puncta. Scale bar, 10  $\mu$ m.

**D** Quantification of synapse numbers in CD38 AS-cKO<sup>P10</sup> mPFC ( $n = 4$  animals per condition, Kruskal–Wallis test followed by Dunn’s test).

Data information: Data represent means  $\pm$  SEM. N.S., no significance; \* $P < 0.05$ , \*\* $P < 0.01$ , \*\*\* $P < 0.001$ .

were identified (Table 1). Among these proteins, SPARC-like protein 1 (SPARCL1) promotes synapse formation by interacting with presynaptic neuroligin-1 $\alpha$  and postsynaptic neuroligin-1B (Singh *et al*, 2016). Proteomics analysis showed that SPARCL1 in CD38 KO-ACM was reduced to  $58.3 \pm 6.6\%$  of that in WT-ACM (Table 1). We further examined the amount of intracellular and extracellular SPARCL1 and other synaptogenesis-related secreted proteins, such as thrombospondin-1 (TSP1; Christopherson *et al*, 2005), and brain-derived neurotrophic factor (BDNF; Park & Poo, 2013), in WT and

CD38 KO astrocytes by western blotting analysis of ACM and cell lysates of these cells. Although TSP1 and BDNF levels in ACM and cell lysate were not different between WT and CD38 KO astrocytes, both extracellular and intracellular SPARCL1 levels in CD38 KO astrocytes were significantly lower than those in WT astrocytes (Fig 4A–C). Next, we investigated SPARCL1 and CD38 expression level in the mPFC of developing brains. Consistent with previous studies in the cortex (Risher *et al*, 2014; Hattori *et al*, 2017), the expression of SPARCL1 and CD38 was developmentally regulated in the postnatal

**Table 1. The proteomics of conditioned media from WT or CD38 KO astrocytes.**

Uni ac No.	Protein	KO ACM/ WT ACM (%)	Variation (%)
Q6GU68	Immunoglobulin superfamily containing leucine-rich repeat protein	38.9	10.02
Q91WP6	Serine protease inhibitor A3N	43.6	6.31
P50608	Fibromodulin	53.1	0
P70663	SPARC-like protein 1	58.3	6.61
Q61702	Inter-alpha-trypsin inhibitor heavy chain H1	59.4	12.94

The table shows extracellular proteins with an abundance ratio of (CD38 KO ACM)/(WT ACM), with  $1.5 >$  or  $< 0.67$ , and an abundance ratio variability (%)  $< 15$  ( $n = 2$  independent cultures from two animals per genotype).

mPFC and peaked at P21 to P28 (Fig 4D–F). Further immunohistochemical analysis demonstrated that SPARCL1 expression was largely restricted to S100 $\beta$ -positive astrocytes in the mPFC at P21 (Fig 4G and H). We found significantly decreased expression of SPARCL1 in astrocytes of CD38 AS-cKO<sup>P10</sup> mice compared to that of ctrl<sup>P10</sup> mice at P21 (Fig 4G and H). In contrast, SPARCL1 expression in NeuN-positive neurons was not altered in the CD38 AS-cKO<sup>P10</sup> mice (Fig 4H).

Since it has been reported that astroglial SPARCL1 promotes excitatory synapse formation in cultured neurons (Blakely *et al.*, 2015; Gan & Sudhof, 2020), we examined the effect of SPARCL1 knockdown on synaptogenesis in cultured astrocytes. Transfection of SPARCL1 siRNA strongly reduced SPARCL1 protein in both the cell lysate and ACM of astrocytes (Appendix Fig S6A). ACM of SPARCL1-knockdown cells significantly decreased synapse formation of cortical neurons (Appendix Fig S6B and C). To confirm the involvement of SPARCL1 in CD38-mediated synaptogenesis, we evaluated synaptogenesis in neurons treated with recombinant SPARCL1 protein in CD38 KO-ACM. Treatment with SPARCL1 significantly increased the decreased synapses in neurons cultured with CD38 KO-ACM up to  $87.1\% \pm 0.09$  of those with WT ACM (Fig 5A and B). We further tested whether injection of SPARCL1 into the developing mPFC recovered the decreased synapse number in CD38 AS-cKO<sup>P10</sup> mice. We injected recombinant SPARCL1 protein into Layer II/III of the CD38 AS-cKO<sup>P10</sup> mPFC at P15, and then the synapse number at P18 was examined by immunohistochemistry of VGlut1 and PSD95. Quantitative analysis of colocalized VGlut1 and PSD95 synaptic puncta revealed that the decreased excitatory synapses in CD38 AS-cKO<sup>P10</sup> mice were significantly increased up to  $87.9 \pm 4.6\%$  of saline-injected ctrl<sup>P10</sup> mice by SPARCL1 injection (Fig 5C and D). These results show that CD38 increases excitatory synapse formation mainly by promoting the release of SPARCL1 from astrocytes.

#### **cADPR/calcium signaling regulates release of SPARCL1 from astrocytes**

CD38 catalyzes the synthesis of a calcium messenger cADPR, which releases Ca<sup>2+</sup> from intracellular stores (Banerjee *et al.*, 2008), and CD38/cADPR/Calcium signaling is involved in astrocytic production of extracellular mitochondria (Hayakawa *et al.*, 2016). Therefore, we assessed the role of this pathway in the release of extracellular

SPARCL1 from astrocytes. We used 8-Bromo-cADPR, a cADPR antagonist; 2APB, an IP<sub>3</sub> inhibitor; and dantrolene, a ryanodine receptor (RYR) inhibitor, to block cADPR/calcium signaling (Fig 6A). All of these compounds significantly decreased the release of SPARCL1 from astrocytes (Fig 6B and C). In contrast, they did not change the expression of intracellular SPARCL1 in astrocytes (Fig 6B and D), indicating that CD38/cADPR/calcium signaling is involved in the release of SPARCL1 from astrocytes. Previous RNA-seq analysis of astrocytes sorted from the hippocampus and striatum suggests expression of RYR1, 2, and 3 in these cells (Chai *et al.*, 2017). Therefore, we examined mRNA expression of RYRs in the mPFC astrocytes of ctrl<sup>P10</sup> and CD38 AS-cKO<sup>P10</sup> mice at P20 using the cells isolated by MACS as shown in Fig EV1. Although RYR1 and 3 were undetectable in these cells, RYR2 was expressed slightly lower level in the ACSA2 positive astrocytes than those in the ACSA2 negative cells (Fig 6E). Finally, we performed bulk RNA-seq analysis of astrocytes from WT and CD38 KO mice at P1 ( $n = 2$  independent cultures per genotype). The RNA-seq analysis revealed altered gene expression profile in astrocytes by deletion of CD38 (Fig 7A). We performed Kyoto Encyclopedia and Genes and Genomes (KEGG) pathway analysis on 289 decreased and 471 increased genes in CD38 KO astrocytes ( $\log_2$  fold change  $< -0.57$  or  $> 0.57$ ; FPKM  $> 3$ ; FDR  $< 0.05$ ) from the RNA-seq data, ranked by  $P$  value (Fig 7B and C, and Datasets EV2 and EV3). We found that the calcium signaling pathway was significantly downregulated in CD38 KO astrocytes (Fig 7B). In contrast, most of the pathways upregulated in CD38 KO astrocytes were related to inflammatory response (Fig 7C).

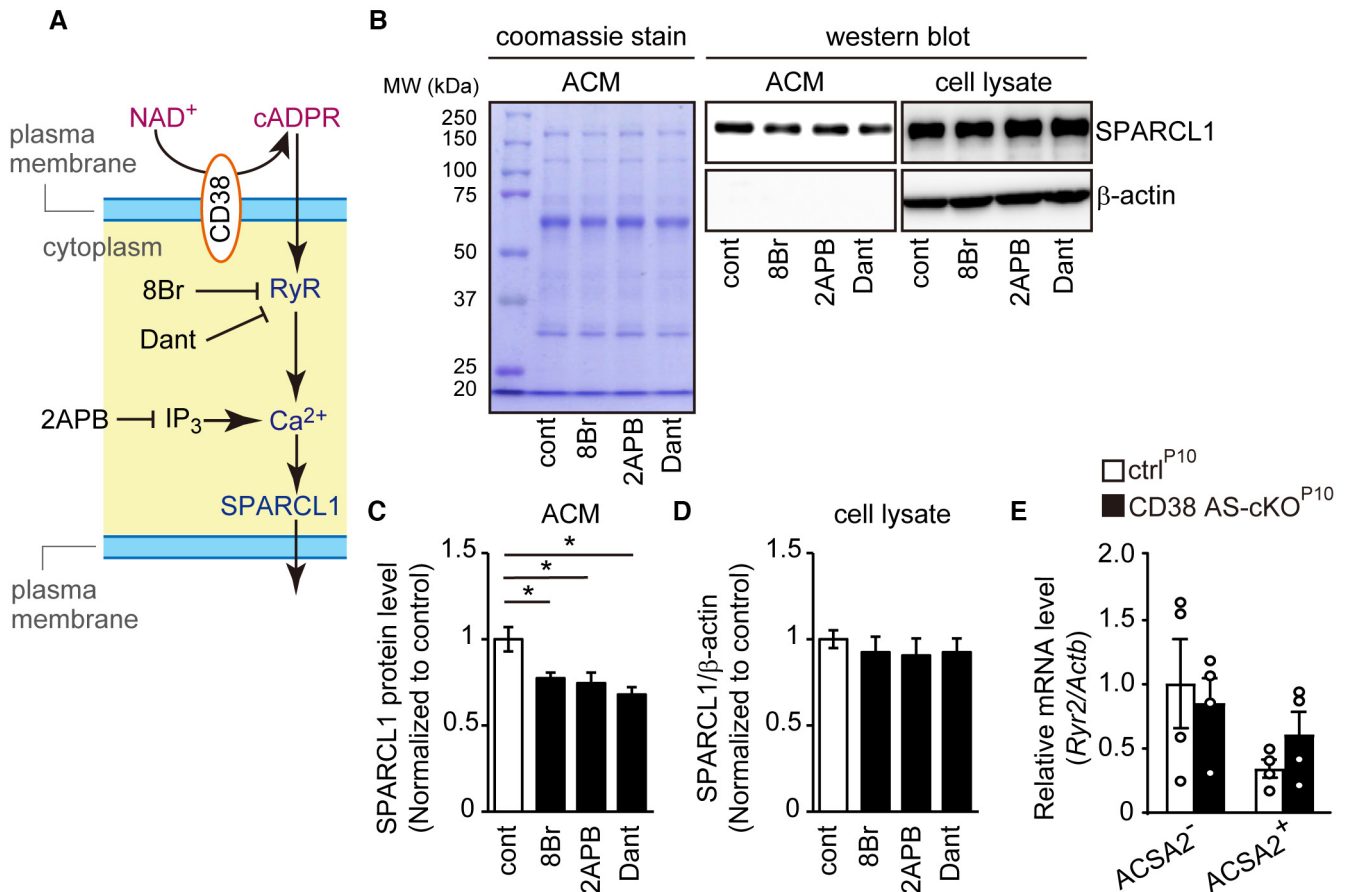
## **Discussion**

In this study, we clarified the role of astroglial CD38 in social behavior. We fortuitously found astroglial CD38 to specifically regulate social memory in the postnatal brain and synapse formation in the mPFC and hippocampus. CD38 regulated SPARCL1 expression and secretion in astrocytes, contributing to synaptogenesis in excitatory neurons. Moreover, SPARCL1 secretion from astrocytes was regulated by CD38/cADPR/calcium signaling. These results demonstrate that astroglial CD38 plays a pivotal role in social memory by regulating the formation of neural circuits in the developing brain.

#### **Regulation of social memory by astroglial CD38**

Multiple studies have reported the involvement of astrocytes in cognitive processes such as learning, memory, and attention by manipulating astrocyte-specific molecules (Augusto-Oliveira *et al.*, 2020). For the first time, we demonstrated the involvement of astrocyte in social memory. Although the deletion of astroglial CD38 from P10 completely impaired social memory, its deletion from P42 did not cause social memory deficits (Fig 1E and I). These results indicate that astroglial CD38 developmentally regulates social memory. Synapse formation occurs from the first to third week of postnatal cortical development, which is concurrent with astrocyte developmental processes including division, expansion, process outgrowth, and release of synapse-regulating molecules (Farhy-Tselnick & Allen, 2018). Expression levels of CD38 and SPARCL1 peaked during this period (Fig 4D–F), and impaired development of astrocytes





such as decreased expression of GFAP, s100β, and Cx43 was observed in CD38 AS-cKO<sup>P10</sup> mice at P21 (Fig EV2). Furthermore, the number of synapses in the mPFC was decreased in CD38 AS-cKO<sup>P10</sup> mice but not in CD38 AS-cKO<sup>P42</sup> mice (Fig 3A–D and Appendix Fig S3). Therefore, it is reasonable to consider that astroglial CD38 plays a pivotal role in social memory neural circuit formation by promoting synapse formation in the developing brain.

The number of excitatory synapse was significantly decreased in the pyramidal neurons of the mPFC as well as hippocampal CA1 and CA2 (Figs 3 and EV5). Previous studies have demonstrated the involvement of mPFC and ventral CA1 and dorsal CA2 of the hippocampus in social memory (Hitti & Siegelbaum, 2014; Okuyama et al, 2016; Xing et al, 2021). The decreased number of synapse in these critical regions likely impaired the social memory in CD38 AS-

cKO<sup>P10</sup> mice. Although the involvement of the mPFC in social behavior, emotion, and cognitive processes has been shown (Chini & Hanganu-Opatz, 2021), we observed specific impairment in social memory due to deletion of astroglial CD38 in the postnatal brain (Fig 1). The synapse number in the mPFC of CD38 AS-cKO<sup>P10</sup> mice was reduced to 82.2% of those in control mice (Fig 3). This slight synaptic reduction in the mPFC of CD38 AS-cKO<sup>P10</sup> mice seems insufficient to cause mPFC-related behavioral impairment, as compared to chemogenetic inhibition of neurons in the previous study (Xing et al, 2021). However, numbers of synapses in the hippocampal CA1 and CA2 of CD38 AS-cKO<sup>P10</sup> mice were also reduced to 78.9 and 74.3% of control levels, respectively (Fig EV5). This slight synaptic reduction in several critical areas of social memory may account for the specific impairment of the behavior. In addition,

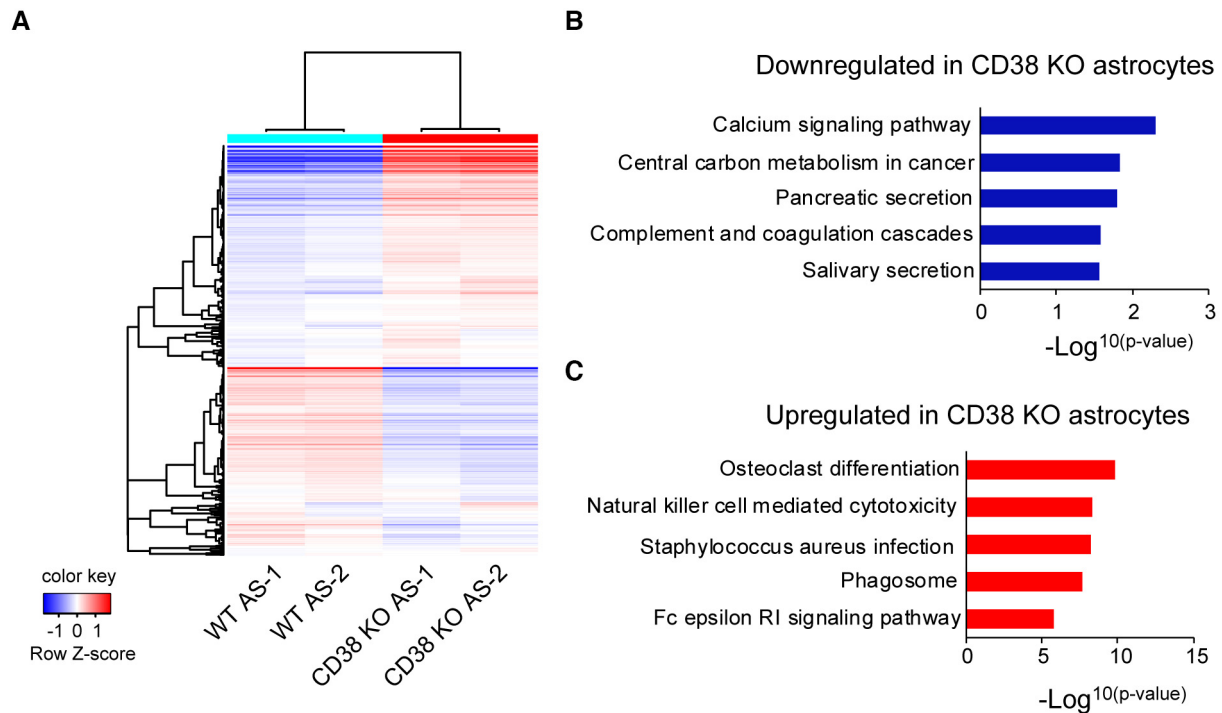


**Figure 7. Transcriptome analyses reveals altered calcium signaling pathway in CD38 KO astrocytes.**

**A** Heat maps of RNA-seq data from WT and CD38 KO cultured astrocytes. Genes and samples were clustered using correlation distance with complete linkage.  
**B, C** Graph depicting top ranked KEGG terms by gene ontology analysis of down- and upregulated genes ( $\log_2$  fold change  $< -0.57$  or  $> 0.57$ ; FPKM  $> 3$ ; FDR  $< 0.05$ ) in CD38 KO astrocytes ( $n = 2$  independent cultures from two animals per genotype). The significance of enrichment in KEGG pathway analyses was calculated using the  $P$  value function obtained from a modified Fisher's exact test using the DAVID database.

critical period for specific neural circuit formation is reported to be different in the postnatal mPFC (Klune *et al.*, 2021). Although the critical period of the social memory circuit has not been clarified, spatiotemporal expression of astroglial CD38 may overlap with critical region and timing of social memory neural circuit formation. However, the deletion of astroglial CD38 may affect other memory functions. As the hippocampus is a central region for coding spatial, temporal, and episodic memory, CA2 is required for social memory formation and spatial memory (Kay *et al.*, 2016). Moreover, constitutive CD38 KO mice exhibit memory deficits in the fear conditioning and Morris water maze tests (Kim *et al.*, 2016; Martucci *et al.*, 2019). Further studies are necessary to clarify the involvement of astroglial CD38 in other functions of memory.

Consistent with previous study (Kim *et al.*, 2016), constitutive CD38 KO mice exhibited impairment of both social memory and social preference (Fig EV3B and C), whereas CD38 AS-cKO<sup>P10</sup> mice showed specific impairment of social memory (Fig 1A–C). This difference in social behavior phenotype is likely due to oxytocin level; the plasma oxytocin level is significantly low in constitutive CD38 KO mice (Jin *et al.*, 2007) but not in CD38 AS-cKO<sup>P10</sup> mice (Fig EV4J). Oxytocin administration recovers impairment of social preference (Sala *et al.*, 2013) and is also involved in pup retrieval behavior, tail suspension test and sucrose preference test (Cherepanov *et al.*, 2017). In addition, although the degree of synaptic reduction in constitutive CD38 KO (Appendix Fig S4D) and CD38 AS-cKO<sup>P10</sup> mice (Fig 3D) was similar, a slight difference in neurons

phenotypes was noted between these mice, such as reduction in VGlut1 puncta (Appendix Fig S4B) and primary dendrite length (Appendix Fig S1B and D) in constitutive CD38 KO mice. Neuronal CD38 or astroglial CD38 expressed before P10 may be involved in these difference. Because CD38 is expressed in neurons in the postnatal cortex and constitutive CD38 KO mice start to show impaired development of astrocytes and oligodendrocytes from P1 (Hattori *et al.*, 2017).

#### Regulation of synapse formation by astroglial CD38

A previous study has demonstrated the role of SPARCL1 in promoting excitatory synapse formation (Gan & Sudhof, 2020). In this study, we observed that treatment with SPARCL1 almost recovered the decreased excitatory synapse number, which was caused by the deletion of astroglial CD38 *in vitro* and *in vivo* (Fig 5). Furthermore, SPARCL1 was specifically expressed in the astrocytes of the postnatal mPFC (Fig 4G and H), similar to that in the visual cortex (Risher *et al.*, 2014). Levels of SPARCL1 and CD38 expression were similarly regulated in the postnatal mPFC (Fig 4D–F). Therefore, SPARCL1 likely plays a major role in astroglial CD38-mediated synapse formation in the developing brain. However, treatment with recombinant SPARCL1 did not fully recover the impaired synapse formation caused by the deletion of astroglial CD38 (Fig 5). The recovered levels of synapse formation by SPARCL1 were still lower than those of neurons with WT ACM (Fig 5B) or ctrl<sup>P10</sup> mice injected with

saline (Fig 5D). These results suggest that other known and unknown synaptogenic factors are involved in the CD38-mediated synapse formation. Significant up- or downregulated known synapse formation-mediating molecules, except SPARCL1, were not found in the proteomics of CD38 KO ACM (Dataset EV1). This may be due to fewer number of proteins identified by our proteomics than those in other similar studies (Dowell *et al*, 2009; Greco *et al*, 2010). In fact, known astrocytic synaptogenic molecules, such as TGF- $\beta$ 1 and Glypican 4/6 (Baldwin & Eroglu, 2017), were not detected in our proteomics. Therefore, we possibly did not detect all the secreted proteins, which were affected by the deletion of astroglial CD38. Moreover, in this study we did not examine *in vivo* secretion of the synaptogenic factors and their effect on social memory behavior in our mouse model. Further studies are required to identify astrocyte-derived factors, which are involved in CD38-mediated synaptogenesis of social memory circuit formation.

Blocking of IP<sub>3</sub> or cADPR/calcium signaling was found to decrease the secretion of SPARCL1 from astrocytes (Fig 6B and C). Furthermore, RNA-seq analysis revealed downregulated calcium signaling pathways in CD38 KO astrocytes (Fig 7B). These results indicate the involvement of calcium signaling in SPARCL1 secretion. CD38 produces cADPR from NAD<sup>+</sup> and the suppression of CD38 expression downregulates astrocytic cADPR/calcium signaling (Banerjee *et al*, 2008). Thus, the decreased extracellular SPARCL1 in CD38 KO ACM is likely attributed to the downregulation of astrocytic cADPR/calcium pathway. Furthermore, intracellular SPARCL1 expression was significantly decreased in CD38 KO astrocytes (Fig 4C). In addition to the decreased release from astrocytes, this also contributed to the decreased extracellular SPARCL1 levels in CD38 KO astrocytes. However, blocking of the cADPR/calcium pathway did not decrease its expression (Fig 6D). In this study, the pathway was blocked for 48 h in astrocytes. Continuous long-term suppression of this signaling pathway may be necessary for downregulating SPARCL1 expression. Otherwise, elevation in NAD<sup>+</sup> levels by the deletion of CD38 may be involved in the suppression of SPARCL1 expression.

In conclusion, astroglial CD38 developmentally regulates social memory and neural circuit formation in the developing brain by promoting synaptogenesis via SPARCL1. The identification of a novel astroglial molecule that mediates social memory without affecting other social behaviors may provide potential targets for the treatment of neurological conditions with social memory deficits, such as autism.

## Materials and Methods

### Animals

All animal experiments were approved by the Animal Care and Use Committee of Kanazawa University (AP-194042). *Cd38<sup>flox/flox</sup>* mice were obtained from Akira Sugawara, Tohoku University. *Glast<sup>CreERT2/+</sup>* mice were obtained from Magdalena Götz, GSF-National Research Center for Environment and Health (Mori *et al*, 2006). For Cre-lox experiments, *Cd38<sup>flox/flox</sup>:Glast<sup>CreERT2/+</sup>* were crossed with *Cd38<sup>flox/flox</sup>:Glast<sup>+/+</sup>*. Male *Cd38<sup>flox/flox</sup>:Glast<sup>CreERT2/+</sup>* and *Cd38<sup>flox/flox</sup>:Glast<sup>+/+</sup>* were injected with tamoxifen (20 mg/kg; T-5648, Sigma-Aldrich, St. Louis, MO, USA) intraperitoneally once a

day for 5 consecutive days from P10 or P42, a protocol previously demonstrated to induce efficient recombination (Lizen *et al*, 2015). CD38 KO mice were generated as described previously (Kato *et al*, 1999). All mice were maintained by breeding to ICR mice and housed in 345 × 168 × 140 mm cages in a temperature-controlled room (24–25°C) with 12-h light–dark cycles. Food and water were available *ad libitum*. Sample size for each experiment was determined based on our previous studies. Animals were randomly allocated for experimental groups.

### Three chamber test

The three chamber social apparatus was a (90 × 50 × 30 cm) plexi-glass box, which was divided into three equal size compartments by two transparent partitions. At the floor level of each partition, there was a square opening (5 × 5 cm) located in the center, allowing access into each chamber. Two small, round wire cages were put in the diagonal corner of the apparatus for enclosing a stranger mouse or a similar size ball and two weighted bottles were placed on the top of the cages to prevent the test mice from climbing over the wire cages. The test was designed in accordance with previous study (Zhang *et al*, 2016). The day before the test, all the test mice were habituated to the apparatus for 20 min with the two empty cages inside and all the stranger mice were habituated inside the wire cages for 20 min at a separate time. On the test day, after a 10-min habituation period, a stranger mouse was placed into one of the two wire cages while an inanimate ball was placed into the other. Then, the subject mouse was placed in the center, and allowed to freely explore the chamber for 5 min. The subject had the choice between a stranger mouse and an inanimate ball in this phase (sociability phase). Immediately after the sociability phase, the inanimate ball was replaced by a second stranger mouse, and the subject was allowed to freely explore the chamber for another 5 min. Thus, the subject would now have the choice between the mouse that the subject had already encountered and a new stranger mouse (preference for social novelty phase). After an interval of 30 min, the second stranger mouse was replaced by a third stranger mouse, and the subject was allowed to freely explore the chamber for 5 min again. Now it had the choice between familiar stranger 1 that it had already encountered 30 min before and the unfamiliar stranger 3 (social memory phase). Interaction time was scored when the subject was sniffing towards the cages within 2 cm. The location of the stranger 1 was alternated between tests. All the stranger mice used in the test were age- and gender-matched ICR mice. Researchers were blind to genotypes during experiments. Behavior was recorded on video-source and was analyzed using ANY-Maze behavioral tracking software (Stoelting Co.).

### Primary astrocyte culture

Astrocytes were isolated from the cerebral cortex of P1 to P3 neonatal mice following methods previously described (Takarada-Iemata *et al*, 2014). Briefly, cerebral cortices were harvested from neonatal mice. The brain tissue was then digested at 37°C in 4-(2-hydroxyethyl)-1-piperazineethanesulfonic acid (HEPES)-buffered saline containing Dispase II (383-02281, 2 mg/ml; Wako). Cells were plated in PDL-coated flasks (356537, Corning, Corning, NY, USA) in D-MEM (044-29765, WAKO) supplemented with 10% fetal bovine serum (172012, Sigma-Aldrich). After 10 days of cultivation,

microglial cells and oligodendrocytes were removed by aspiration following 20 h shaking and the adherent cell population was collected after being detached using 0.05% trypsin–EDTA (15400054, Thermo Fisher Scientific). Collected cells were plated at  $1 \times 10^5$  cells/cm<sup>2</sup> density. The next day the medium was changed in order to remove cell debris and loosely attached cells. Medium was changed every 3 days.

### Primary neuron culture

Primary cortical neurons were prepared from embryonic day 18 BL6 male and female mice with nerve cell culture system 291-78001 (FUJIFILM Wako Chemicals Co. Ltd, Tokyo, Japan). Four well chamber slides (177437, Thermo Fischer Scientific) were coated by incubating for 12 h with filter sterilized poly-L-lysine (P8920, Sigma-Aldrich; 100 µg/ml) in borate buffer (boic acid 3.1 g/l, borax 4.8 g/l in water). Then, they were washed with sterile water and dried before use. Neurons were plated on the chamber slides at a density of  $1 \times 10^5$  cells per well and cultured in Neurobasal medium (21103049, Thermo Fischer Scientific) with 5% FBS, 2% B27 supplement (A3582801, Thermo Fischer Scientific), 100 µg/ml Penicillin–Streptomycin (168-23191, WAKO) and 0.5 mM L-glutamine (076-00521, WAKO).

### Primary neuron culture with conditioned medium from astrocyte cultures

Astrocytes were isolated from wild-type (WT) or CD38 KO neonatal male and female mice as described above. After 9 days of cultivation, cells were replated in 10 cm diameter dishes at the density of  $5 \times 10^5$  cells per dish and cultured for 48 h. Then all of the media was replaced with Neurobasal medium supplemented with 2% B27 supplement and 0.5 mM L-glutamine after washing with phosphate-buffer saline (PBS) three times. The media were harvested 24 h after replacement, and filtrated by Millex-GP filter (SLGPR33RS, Merck Millipore) and centrifuged at 3,000 g for 3 min to remove cellular debris. 500 µl of the ACM was concentrated with Amicon Ultra 10 kDa (UFC501008, Merck) following the manufacture's protocol. Total protein concentration was determined by Bradford assay and protein concentration of each ACM sample was adjusted by adding Neurobasal medium supplemented with 2% B27 supplement and 0.5 mM L-glutamine. Primary neuron cultures were isolated as described above and plated on 4 well chamber slide coated with poly-L-lysine. Three days after plating, cells were cultured with 5 µM AraC (C6645, Sigma-Aldrich) for 24 h. Four days after plating, half of the media were replaced with ACM. At day 9, half of the medium was replaced with ACM again. The neurons were cultured with or without SPARCL1 recombinant protein (80 nM, ATGP3891, NKMAX) from day 8 to day 14 as previously done (Singh *et al*, 2016). Cells were fixed by 4% paraformaldehyde for immunostaining at day 14. The purity of neurons was determined by immunocytochemistry using anti-NeuN antibody. The percentage of neurons in WT and CD38 KO ACM was  $98.2 \pm 0.9$  and  $98.5 \pm 0.2\%$ , respectively.

### Golgi staining

Male mice (4 ctrl<sup>P10</sup>, 4 CD38 AS-cKO<sup>P10</sup>, 4 WT and 4 CD38 KO) aged 10 weeks were used. Brains were removed and Golgi-Cox staining

was performed using an FD Rapid GolgiStain Kit (PK401, FD Neuro-Technologies) according to the manufacturer's instructions. Unfixed brain samples were processed as previously reported (Koyama *et al*, 2013). The coronal brain blocks were immersed in a solution of equal parts Solution A and B at room temperature for 2 weeks and then soaked in Solution C at 4°C for 48 h. After freezing with dry-ice powder, the brain samples were sliced into 250 µm pieces at –22°C using a cryostat microtome. Each frozen section was mounted with Solution C on a 0.5% gelatin-coated glass slide. Slides were allowed to dry naturally at room temperature and were then stained with a mixture (Solution D: Solution E: DW; 1:1:2) for 5 min, after which the slides were rinsed in distilled water twice for 4 min each. Slides were dehydrated in an ascending ethanol series and then sealed with Entellan (Merck) through xylene. The preparations were observed in detail with a BZ-9000 digital microscope (Keyence Corporation).

To assess dendritic morphology, low magnification (20× lens) images (Z-stack with 1 µm intervals) of pyramidal neurons, with cell bodies located in Layer II/III of the mPFC, were randomly captured. Captured images from ctrl<sup>P10</sup>, CD38 AS-cKO<sup>P10</sup>, WT, and CD38 KO neurons were manually traced using Simple Neurite Tracer plug-in (SNT) from FIJI (Arshadi *et al*, 2021). Total length and number of all the dendrites and primary dendrites were measured with SNT.

To assess dendritic spine morphology, high magnification (63× lens) images (Z-stack with 0.2 µm intervals) of pyramidal neurons were captured. The density of spines was quantified by counting the number of spines on the following segments: dendritic segments (50–100 µm) of apical dendrites located farther than 50 µm from cell soma of ctrl<sup>P10</sup>, CD38 AS-cKO<sup>P10</sup>, WT, and CD38 KO neurons. The spines were classified based on their morphology such as a mushroom type (diameter of the spine head was larger than that of the spine neck), thin type (diameter of the spine head was equal to that of the spine neck), stubby spines (no neck), and ramified spines (two heads).

### Western blot analyses

Conditioned media from astrocytes were collected at 5 DIV and filtrated with Millex-GP filter (SLGPR33RS, Merck). ACM was concentrated with Amicon Ultra 10 kDa (UFC501008) following the manufacture's protocol. Total protein concentration was determined by Bradford assay. Cells and brain samples (mPFC) were homogenized and solubilized in a buffer containing 1% NP40, 0.1% sodium dodecyl sulfate, and 0.2% deoxycholate. Lysates and ACM were boiled for 5 min with sodium dodecyl sulfate (SDS) sample buffer. Equal amount of protein was subjected to SDS-polyacrylamide gel electrophoresis (SDS-PAGE) and proteins were transferred to polyvinylidene fluoride (PVDF) membranes. After blocking in 5% skimmed milk, the membrane was incubated for 12 h at 4°C with the primary antibody: anti-VGluT1 (AB5905, Millipore, 1:2,000), anti-PSD95 (51-6900, Thermo Fischer Scientific, 1:500), anti-CD38 (AF4947, R&D Systems, 1:300), anti-β-actin (013-24553, WAKO, 1:2,000), anti-SPARCL1 (AF2836, R&D Systems, 1:2,000), anti-TSP1 (sc-59887, Santa Cruz, 1:500), anti-BDNF (ab108319, Abcam, 1:2,000), anti-GFAP (G9269, SIGMA, 1:2,000), anti-Cx43 (MAB3068, Merck Millipore, 1:200), anti-NDRG2 (sc-19468, Santa Cruz Biotechnology, 1:500), and anti-MAG (sc-15324, Santa Cruz Biotechnology,



1:500). The membrane was incubated for 1 h at room temperature with anti-rabbit, mouse or goat horseradish peroxidase (HRP)-linked IgG (sc-2357, sc-516102, sc-2354, Santa Cruz Biotechnology, 1:5,000). Immunoreactivity was detected using an enhanced chemiluminescence system (ELLUF0100, Merck). Densitometric quantification was performed using ImageJ 1.52 software (<https://imagej.nih.gov/ij/>). For Coomassie Blue staining gels were stained with staining solution (0.2% of Coomassie Blue, 60% of methanol, and 12% of acetic acid in distilled water) for overnight. After rinsing with water, gels were destained with solution (10% of methanol and 10% of acetic acid in distilled water). Quantified density of proteins in ACM was normalized by the density of the total protein by Coomassie Blue staining of gels.

### Immunohistochemistry and synaptic puncta analysis

The brains were removed from the mice after perfusion with 4% paraformaldehyde (PFA). The brains were fixed with 4% PFA in PBS at 4°C overnight and then cryoprotected with 30% sucrose in PBS overnight. Cortical sections (20- $\mu$ m thick sections) were cut on a cryostat (Leica CM1950, Leica). Sections were washed and permeabilized in PBS with 0.3% Triton-X 100 three times at room temperature. Sections were blocked in 3% Bovine Serum Albumin (BSA, 015-21274, WAKO) in PBS for 1 h at room temperature. Primary antibodies against GFAP (G9269, SIGMA, 1:2,000), NDRG2 (sc-19468, Santa Cruz Biotechnology, 1:500), VGlut1 (AB5905, Millipore, 1:2,000), VGlut2 (AB2251-I, Millipore, 1:2,000), PSD95 (51-6900, Thermo Fischer Scientific, 1:500), S100 $\beta$  (S2532, Sigma-Aldrich, 1:300), SOX9 (AF3075, R&D Systems, 1:300), NenN (MAB377, Millipore, 1:500), MBP (MAB386, Millipore, 1:300), and SPARCL1 (AF2836, R&D Systems, 1:500) were diluted in 3% BSA containing PBS. Sections were incubated with primary antibodies overnight at 4°C. Alexa488-conjugated anti-guinea pig IgG (ab150185, Abcam, 1:300), Cy3-conjugated anti-rabbit IgG (711-165-152, Jackson Laboratory, 1:300), FITC-conjugated anti-goat IgG (ab7121, Abcam, 1:300), Cy3-conjugated anti-mouse IgG (715-165-150, Jackson Laboratory, 1:300), or Alexa488-conjugated anti-rat IgG (A21208, Thermo Fischer Scientific, 1:300) was used to visualize immunolabeling. Slides were mounted in Vectashield with DAPI and images were acquired on a laser scanning confocal microscope (Dragonfly; Andor). Four animals/genotype were stained with pre- (VGlut1) and postsynaptic (PSD95) marker pairs as described previously (Risher *et al*, 2014). Three independent coronal sections per each mouse, which contain the mPFC (Bregma 2.0 to 2.8 mm), CA1, and CA2 (Bregma -1.7 to -2.1 mm) were used for analyses. 5- $\mu$ m thick confocal z-stacks (optical section depth 0.33  $\mu$ m, 15 sections/z-stack, scanned area 0.04 mm<sup>2</sup>) of the layer II/III in the prelimbic region of the mPFC and the stratum radiatum in the CA1 and CA2 of the hippocampus were imaged with a 63 $\times$ /1.20 W HC PL APO CORR CS2 objective on a Dragonfly confocal laser scanning microscope. Maximum projections of three consecutive optical slices (corresponding to 1  $\mu$ m total depth) were generated from the original z-stack. A total of five confocal z-stacks per animal were analyzed for blind analysis using ImageJ 1.52 software. 1- $\mu$ m thick maximum projections were separated into green and red channels and thresholded to detect discrete puncta without introducing noise. Density of thresholded pre- and postsynaptic markers was measured using the Measure Particles function where a puncta size was defined for each marker (Vglut1 = 0.1–infinity;

PSD95 = 0.1–infinity). The colocalization of puncta was quantified using the Image Calculator function applied to thresholded pre- and postsynaptic images. The synapse and terminal densities were calculated by taking the total puncta area and dividing it by the total area of the field of view. Densities for ctrl<sup>P10</sup> were averaged, then all image values were converted to ratio to the calculated control<sup>P10</sup> average.

### Immunocytochemistry

Immunofluorescent staining of primary cultures was performed as previously described (Hattori *et al*, 2007). Briefly, cells were fixed with 4% PFA for 10 min, permeabilized with 0.1% Triton-X for 10 min, and blocked with 3% BSA for 1 h at room temperature. After overnight incubations with antibodies against VGlut1 (1:3,000) and PSD95 (1:1,000) at 4°C, the cells were incubated with Alexa-488 and Cy3-conjugated secondary antibodies and DAPI for 1 h at room temperature. Imaging was performed at 63 $\times$  magnification on a laser scanning confocal microscope (Dragonfly). Synaptic puncta were counted along well-isolated primary dendrites (100  $\mu$ m dendritic segments) using a 63 $\times$  lens on a fluorescence microscope. The number of colocalized puncta was calculated by ImageJ 1.52 as described above. All image values were converted to ratio to the calculated WT ACM average.

### Comparative shotgun proteomics using nano-liquid chromatography mass spectrometry

After the WT and CD38 KO astrocytes reached confluency at 7 DIV, cells were washed three times with PBS and 10 ml of neurobasal medium was added. After 24 h, astrocyte conditioned medium and control neurobasal medium were collected and filtrated with Millex-GP filter. The conditioned medium was precipitated using trichloroacetic acid (TCA) with the carrier sodium lauroyl sarcosinate (NLS). The protein pellets were resuspended in the mixed buffer of 6 M urea and 50 mM triethylammonium bicarbonate (TEAB) in pH 8.5. After quantification of protein concentration by BCA method, all proteins (10  $\mu$ g) were adjusted to a final volume of 10  $\mu$ l. Comparative shotgun proteomics were performed as previously described (Shinohara *et al*, 2021). Briefly, these proteins were reduced, by tris(2-carboxyethyl phosphine (TCEP)), alkylated by iodoacetamide (IAA), and digested by trypsin. The trypsin-digested peptides were purified and separated on the LC system (EASY-nLC 1200; Thermo Fisher Scientific). The peptide ions were detected using MS (Orbitrap QE plus MS; Thermo Fisher Scientific). The MS/MS searches were carried out using SEQUEST HT search algorithms against the Mus Musculus (Swiss prot. Tax ID 10090) protein database (2017-6-7) using Proteome Discoverer (PD) 2.2 (Version 2.2.0.388; Thermo Fisher Scientific). Label-free quantification was also performed with PD 2.2 using precursor ions quantifier nodes. Normalization of the abundances was performed using total peptide amount mode. Among identified proteins in WT and CD38 KO ACM, Proteins with abundance Ratio: (CD38 KO ACM)/(WT ACM) with 1.5 > or < 0.67 and abundance Ratio Variability (%) < 15 were subjected to following a gene ontology (GO) analysis using the online version of DAVID Bioinformatics Resources 6.8 (<https://david.ncifcrf.gov/home.jsp>). A functional annotation analysis was performed with the gene ontology tool (GOTERM\_CC\_ALL) using the UniProt Accession numbers of the proteins and extracellular



proteins were shown in Table 1. The list of the identified proteins in WT and CD38 KO ACM were shown in Dataset EV1.

### In vivo SPARCL1 injections

P15 ctrl<sup>P10</sup>, CD38 AS-cKO<sup>P10</sup> littermate mice were deeply anesthetized with intraperitoneal injection of a mixture of anesthetic, muscle relaxant, analgesic and sedative such as medetomidine (0.3 mg/kg; Domitor®; Nippon Zenyaku Kogyo), butorphanol (5.0 mg/kg; Vetorphale®; Meiji Seika Pharma), and midazolam (4.0 mg/kg; Midazolam Sandoz®; Sandoz). With Neuros Syringe (65460-05, Hamilton) mice were stereotactically injected with PBS (600 nl) or recombinant SPARCL1 protein (150 ng in PBS, NKMAX) into layer II/III of mPFC (0.3 mm anterior to Bregma, and 0.2 mm right to the midline at a depth of 0.6 mm from brain surface). After 3 days, pups were anesthetized with isoflurane then perfused transcardially with PBS followed by 4% PFA. The brains were fixed with 4% PFA in PBS at 4°C overnight and then cryoprotected with 30% sucrose in PBS overnight. Sections (20 µm) were stained for VGlut1 and PSD95 as described above. Imaging was performed on a laser scanning confocal microscope (Dragonfly) in area mPFC approximately 40–100 µm caudal or rostral to the injected site.

### RNA-seq transcriptome profiling

WT and CD38 KO astrocytes were cultured in the culture media containing 10% fetal bovine serum for 5 days. The cells were washed with PBS three times and then collected. Total RNAs were extracted from the cells using the FASTGene™ RNA Basic Kit (FG-80250, Nippon Genetics Co., Ltd) and used for RNA library preparation using TruSeq Stranded mRNA Sample Preparation Kit (Illumina, Inc.), with polyA selection for ribosomal RNA depletion. The RNA-seq libraries were generated in duplicate from 500 ng of total RNAs extracted from cultured mouse astrocytes. The libraries were sequenced on Illumina HiSeq 2000 to obtain paired-end 101 bp reads for each sample.

RNA-seq reads from mouse cultured astrocytes were aligned to their reference genomes using the STAR v2.7.0f (Dobin et al, 2013). The Ensembl reference genome used was GRCm38.99 (Cunningham et al, 2019). The gene expression profiles were quantified using Cufflinks v2.2.1 (Trapnell et al, 2013) from the aligned RNA-Seq reads with gene annotation information corresponding to the above reference genome. Gene expression levels were given by FPKM, which is normalized by the number of RNA fragments mapped to the reference genome and the total length of all exons in the transcript. For bioinformatic analysis of RNA-seq, gene ontology analysis was performed by creating a pre-ranked list of all detected transcripts, ranked by log<sub>2</sub> fold change < -0.57 or > 0.57 and FDR < 0.05. DAVID, the Database for Annotation, Visualization and Integrated Discovery v6.7 was used to analyze significant changes by KEGG. Significance of enrichment in KEGG pathway analyses was calculated using the *P* value function given from a modified Fisher's exact test by the DAVID database.

### MACS-based astrocyte isolation

After perfusion with ice-cold HBSS, brains at P20 were cut into 1 mm coronal slices and the mPFC and hippocampus were

dissected. The tissue was cut to small pieces and dissociated with the “Neural Tissue Dissociation Kit (P)” (130-092-628, Miltenyi), incubating for 17 min at 37°C. Then, gentle mechanical dissociation was applied after addition of DNase. After 12 min incubation with DNase, more thorough dissociation was applied with fire-polished pipettes. After removal of remaining incompletely dissociated tissue pieces using a 70-µm cell strainer, the enzymatic dissociation reaction was stopped with calcium-containing PBS buffer. The cells were collected by centrifugation and resuspended in 360 µl MACS buffer (0.5% FBS in PBS) and 40 µl of Myelin Removal Beads (130-09096-733, Miltenyi). After 15 min incubation at 4°C, 4 ml of MACS buffer was added and cells were collected by centrifugation. Cells were resuspended in 1 ml of MACS buffer and passed through a pre-equilibrated LS column (130-042-401, Miltenyi) in a magnetic separator (130-090-976, Miltenyi). The column was washed twice with 1 ml of MACS buffer. The cells were collected by centrifugation, resuspended in 40 µl of MACS buffer and 5 µl of FcR blocking reagent. After 10 min incubation at 4°C, 5 µl of magnetic bead-conjugated Anti-ACSA2-antibody (130-097-679, Miltenyi) was added and incubated for 15 min. After adding 1 ml of MACS buffer, cells were collected by centrifugation and resuspended in 500 µl of MACS buffer. The suspension was passed through a pre-equilibrated MS column (130-042-201, Miltenyi) in a magnetic separator. The column was washed three times with 500 µl of MACS buffer and removed from the separator and wash out the purified astrocyte.

### Reverse transcription quantitative polymerase chain reaction (RT-qPCR)

Total RNA was extracted from the cerebral cortex, hippocampus, or cultured cells using the RNeasy Micro Kit (74004, QIAGEN), and cDNA was synthesized using the

Genes	Forward	Reverse
<i>Cd38</i>	5' CGAAGGAGCTTCCAGTAACG 3'	5' TGGCAGGCCTGTAGTTATCC 3'
<i>S100b</i>	5' GGTGACAAGCACAAAGCTGAA 3'	5' GTCCAGCGTCTCCATCACTT 3'
<i>Slc17a7</i>	5' GGTGGAGGGGTCACATAC 3'	5' AGATCCCCGAAGCTGCCATAGA 3'
<i>Iba1</i>	5' CAGCAATGATGAGGATCTGC 3'	5' CCAAGTTTCTCCAGCAITTCG 3'
<i>Pdgfra</i>	5' TCCATGCTAGACTCAGAAGTCA 3'	5' TCCCCGGTGACACAAATTTTTT 3'
<i>Ryr2</i>	5' CCCATGCTGGTGGAGTTCT 3'	5' CAATGCCAGAAAGCTTGA 3'
<i>Actb</i>	5' CGCAGCCACTGTCGAGTC 3'	5' TCATCCATGGCGAACTGGTG 3'

High-Capacity cDNA Reverse Transcription Kit (4368814, Applied Biosystems). Individual cDNA sequences were amplified using the Thunderbird™ SYBR qPCR® Mix (QPS-201, Toyobo) with specific primers. To measure differential expression, the comparative Ct method was used for data analyses in ViiA™ 7 Real-Time PCR system (Applied Biosystems). The primer sequences are listed below.

### Parental retrieval test

The design of the experiments for parental retrieval behavior was described previously (Cherepanov et al, 2017). Virgin males and females of identical genotypes were paired at 56–64 days. A single male and a single female were continuously housed together in a

standard mouse maternity cage from the mating period to the delivery of pups and then to postnatal days 3–5. All family units consisted of a new sire and dam, and their first litter of each genotype was used. Thirty minutes before starting the experiment, the cages with the families were placed in the experimental room for habituation. The sire and dam were placed in a new clean cage with new woodchip bedding for 10 min, while the pups were left in the nest in the original cage. Five pups were randomly selected from the litter and placed individually at a site remote from the nest in the original cage. The sires and dams were returned to the original home cage in the presence of their five biological pups to assess parental behavior. Parental retrieval behavior was evaluated by observing the parent behavior for 10 min following the reunion. Time that each sire or dam returned all the pups completely to the nest was measured. The behavioral tests were carried out in a randomly mixed sequence of the experimental groups.

### Tail suspension test

The tail suspension test was performed as previously described (Cherepanov *et al.*, 2017). After 30 min of habituation in the experimental room, the mice were hanged by fixing their tails by tape to the suspension bar in a plastic suspension box (55 cm height × 60 cm width × 11.5 cm depth). To prevent observing or interacting with each mouse, the mouse was separated with walls but was not able to contact or touch to the walls. Behavior was recorded for 6 min on video-source and was analyzed using ANY-Maze behavioral tracking software (Stoelting Co.). Total immobility time during the last 4 of the 6 min was used. Researchers were blind to genotypes during experiments.

### Sucrose preference

Experimentally naïve, male mice were housed individually and were given a two-bottle choice between distilled water and sucrose solution at a 1% concentration based on our previous results (Cherepanov *et al.*, 2017), which were both available ad libitum. The bottle positions remained constant. Fresh sucrose solution was prepared each day. Cumulative water and sucrose intakes during 24 h were calculated by weighing. Food was provided ad libitum, but food intake was not recorded in this experiment. Sucrose preference was calculated according to formula  $W0 - W1 / ((W0 - W1) + (S0 - S1))$ . Where S0 and W0 are the weight of bottles with sucrose solution and water before the test and S1 and W1 after 24 h after the test. Researchers were blind to genotypes during experiments.

### Elevated plus maze

This test was based on a method that was described previously (Pellow *et al.*, 1985). The maze was made of four black plexiglass arms with two open arms (67 × 7 cm) and two walled arms (67 × 7 × 17 cm) facing each other and connected by a neutral space in the center at 55 cm above the floor under dimly illuminated light (20 lux). The camera-assisted ANY-Maze software automatically tracked the time spent, frequency of entry into each arm in 5 min. Time spent in open, and close arms was evaluated. Researchers were blind to genotypes during experiments.

### Object recognition test

The novel object recognition test was conducted in a big soundproof box (60 × 60 × 100 cm), containing a square, high-walled arena (25 × 25 × 25 cm) at its bottom. Briefly, it consisted of three phases: habituation sessions (day 1 and day 2, no object inside, 20 min/day), training session (day 3, two identical objects placed symmetrically, 10 min), and test session (one familiar object replaced by a novel one, 5 min, session was started immediately after replacing the objects). The two kind of objects used in the test have similar size and smell but differ in shape and texture. The camera-assisted ANY-Maze software automatically tracked the time spent near the objects. The time spent exploring each object was scored when the subject was sniffing towards the object within 2 cm. Researchers were blind to genotypes during experiments.

### Odor discrimination test

All the test mice were single housed before the test. During the test mouse was put in Plexiglas box (90 × 50 × 30 cm). Test session consisted from five trials (each for 5 min) with 5 min paused between them, when mouse was returned to home cage. During sessions 1–4 cotton pad containing neutral odorant (124-03892, R (+)-Limonene, WAKO) was presented. The test mice were allowed to investigate odor. In session 5 another neutral odorant (150-00134, 1-Octanol, WAKO) was presented. Time spent sniffing the odor was measured by manual observation with a stopwatch. Time was only scored when the test mouse was sniffing the swab within 2 cm. Researchers were blind to genotypes during experiments.

### Oxytocin measurement

Thoracotomy was performed under anesthesia by isoflurane, and blood sample was obtained from the ventricle by cardiac puncture. An Oxytocin ELISA kit (ADI-901-153, Enzo Life Sciences) was used for oxytocin analysis by following manufacture's protocol.

### siRNA transfection

We obtained small interference RNA (siRNA) from Sigma. The sequence of the mouse SPARCL1 targeted was as follows: 5'-CTATT CCTGCTGTACGG-3' (SASI\_Mm01\_00135946). We used Stealth RNAi™ siRNA negative control med GC (Thermo Fischer Scientific) as a control siRNA. Transfection of siRNA was performed using RNAimax (Invitrogen) according to the manufacturer's instructions.

### Statistical analyses

Data were analyzed with Statcel 4 (OMS Publishing Inc.) or Prism 8 (GraphPad Software). All data are expressed as mean ± standard error of the mean (SEM), with the number of experiments indicated by (*n*). Analyses used include two-tailed unpaired Student's *t*-test, one-way ANOVA, or two-way ANOVA and appropriate *post hoc* analyses (indicated in Figure Legends). For non-parametric data, the Mann–Whitney *U*-test or the Kruskal–Wallis test with *post hoc* Dunn's test was used. Differences were considered statistically

significant at a  $P$  value of  $< 0.05$ . Summary of statistical analysis for figures are shown in Dataset EV4.

## Data availability

The RNA-seq dataset has been deposited in NCBI GEO database (GSE216887, <https://www.ncbi.nlm.nih.gov/geo/query/acc.cgi?acc=GSE216887>).

**Expanded View** for this article is available [online](#).

## Acknowledgements

We thank Magdalena Götz in Ludwig-Maximilians-Universität München for providing  $\text{Glast}^{\text{CreERT2}}$  mice. We thank Mr. Takashi Tamatani and Ms. Nahoko Okitani for providing technical assistance. This work was supported by Grant-in Aid for Scientific Research (21K06407, 18KK0435 for TH, 18KK0255, 18K06500 for OH, 20K09343 for HI and 21K06406, 18K06463 for MT-I) from the Ministry of Education, Science, Technology, Sports and Culture of Japan, and by Kanazawa University SAKIGAKE Project 2018 and the CHOZEN project.

## Author contributions

**Tsuyoshi Hattori:** Conceptualization; formal analysis; investigation; writing – original draft; project administration; writing – review and editing. **Stanislaw M Cherepanov:** Formal analysis; investigation; writing – original draft. **Ryo Sakaga:** Investigation. **Jurepon Roboon:** Investigation. **Dinh Thi Nguyen:** Investigation. **Hiroshi Ishii:** Investigation. **Mika Takarada-Iemata:** Investigation. **Takumi Nishiuchi:** Investigation; writing – original draft. **Takayuki Kannon:** Formal analysis; investigation. **Kazuyoshi Hosomichi:** Formal analysis; investigation. **Atsushi Tajima:** Formal analysis; investigation. **Yasuhiko Yamamoto:** Resources. **Hiroshi Okamoto:** Resources. **Akira Sugawara:** Resources. **Haruhiro Higashida:** Resources; writing – original draft. **Osamu Hori:** Resources; writing – original draft.

## Disclosure and competing interests statement

The authors declare that they have no conflict of interest.

## References

- Arshadi C, Gunther U, Eddison M, Harrington KIS, Ferreira TA (2021) SNT: a unifying toolbox for quantification of neuronal anatomy. *Nat Methods* 18: 374–377
- Augusto-Oliveira M, Arrifano GP, Takeda PY, Lopes-Araujo A, Santos-Sacramento L, Anthony DC, Verkhatsky A, Crespo-Lopez ME (2020) Astroglia-specific contributions to the regulation of synapses, cognition and behaviour. *Neurosci Biobehav Rev* 118: 331–357
- Baldwin KT, Eroglu C (2017) Molecular mechanisms of astrocyte-induced synaptogenesis. *Curr Opin Neurobiol* 45: 113–120
- Banerjee S, Walseth TF, Borgmann K, Wu L, Bidasee KR, Kannan MS, Ghorpade A (2008) CD38/cyclic ADP-ribose regulates astrocyte calcium signaling: implications for neuroinflammation and HIV-1-associated dementia. *J Neuroimmune Pharmacol* 3: 154–164
- Barak B, Feng G (2016) Neurobiology of social behavior abnormalities in autism and Williams syndrome. *Nat Neurosci* 19: 647–655
- Barca-Mayo O, Pons-Espinal M, Follert P, Armirotti A, Berdondini L, De Pietri TD (2017) Astrocyte deletion of Bmal1 alters daily locomotor activity and cognitive functions via GABA signalling. *Nat Commun* 8: 14336
- Bardehle S, Kruger M, Buggenthin F, Schwausch J, Ninkovic J, Clevers H, Snippert HJ, Theis FJ, Meyer-Luehmann M, Bechmann I et al (2013) Live imaging of astrocyte responses to acute injury reveals selective juxtavascular proliferation. *Nat Neurosci* 16: 580–586
- Billeke P, Aboitiz F (2013) Social cognition in schizophrenia: from social stimuli processing to social engagement. *Front Psychiatry* 4: 4
- Blakely PK, Hussain S, Carlin LE, Irani DN (2015) Astrocyte matricellular proteins that control excitatory synaptogenesis are regulated by inflammatory cytokines and correlate with paralysis severity during experimental autoimmune encephalomyelitis. *Front Neurosci* 9: 344
- Chai H, Diaz-Castro B, Shigetomi E, Monte E, Oceau JC, Yu X, Cohn W, Rajendran PS, Vondriska TM, Whitelegge JP et al (2017) Neural circuit-specialized astrocytes: transcriptomic, proteomic, morphological, and functional evidence. *Neuron* 95: 531–549
- Chao HT, Zoghbi HY, Rosenmund C (2007) MeCP2 controls excitatory synaptic strength by regulating glutamatergic synapse number. *Neuron* 56: 58–65
- Chen P, Hong W (2018) Neural circuit mechanisms of social behavior. *Neuron* 98: 16–30
- Cherepanov SM, Akther S, Nishimura T, Shabalova AA, Mizuno A, Ichinose W, Shuto S, Yamamoto Y, Yokoyama S, Higashida H (2017) Effects of three lipidated oxytocin analogs on behavioral deficits in CD38 knockout mice. *Brain Sci* 7: 132
- Chini M, Hanganu-Opatz IL (2021) Prefrontal cortex development in health and disease: lessons from rodents and humans. *Trends Neurosci* 44: 227–240
- Christopherson KS, Ullian EM, Stokes CC, Mallowney CE, Hell JW, Agah A, Lawler J, Moshier DF, Bornstein P, Barres BA (2005) Thrombospondins are astrocyte-secreted proteins that promote CNS synaptogenesis. *Cell* 120: 421–433
- Chung WS, Allen NJ, Eroglu C (2015) Astrocytes control synapse formation, function, and elimination. *Cold Spring Harb Perspect Biol* 7: a020370
- Cunningham F, Achuthan P, Akanni W, Allen J, Amode MR, Armean IM, Bennett R, Bhai J, Billis K, Boddu S et al (2019) Ensembl 2019. *Nucleic Acids Res* 47: D745–D751
- Dobin A, Davis CA, Schlesinger F, Drenkow J, Zaleski C, Jha S, Batut P, Chaisson M, Gingeras TR (2013) STAR: ultrafast universal RNA-seq aligner. *Bioinformatics* 29: 15–21
- Dowell JA, Johnson JA, Li L (2009) Identification of astrocyte secreted proteins with a combination of shotgun proteomics and bioinformatics. *J Proteome Res* 8: 4135–4143
- Farhy-Tselnicker I, Allen NJ (2018) Astrocytes, neurons, synapses: a tripartite view on cortical circuit development. *Neural Dev* 13: 7
- Gan KJ, Sudhof TC (2020) SPARCL1 promotes excitatory but not inhibitory synapse formation and function independent of Neurexins and Neuroligins. *J Neurosci* 40: 8088–8102
- Gerasimenko M, Lopatina O, Shabalova AA, Cherepanov SM, Salmina AB, Yokoyama S, Goto H, Okamoto H, Yamamoto Y, Ishihara K et al (2020) Distinct physical condition and social behavior phenotypes of CD157 and CD38 knockout mice during aging. *PLoS ONE* 15: e0244022
- Greco TM, Seeholzer SH, Mak A, Spruce L, Ischiropoulos H (2010) Quantitative mass spectrometry-based proteomics reveals the dynamic range of primary mouse astrocyte protein secretion. *J Proteome Res* 9: 2764–2774
- Guse AH (2005) Second messenger function and the structure-activity relationship of cyclic adenosine diphosphoribose (cADPR). *FEBS J* 272: 4590–4597
- Guy J, Gan J, Selfridge J, Cobb S, Bird A (2007) Reversal of neurological defects in a mouse model of Rett syndrome. *Science* 315: 1143–1147

- Han X, Chen M, Wang F, Windrem M, Wang S, Shanz S, Xu Q, Oberheim NA, Bekar L, Betstadt S et al (2013) Forebrain engraftment by human glial progenitor cells enhances synaptic plasticity and learning in adult mice. *Cell Stem Cell* 12: 342–355
- Hattori T, Baba K, Matsuzaki S, Honda A, Miyoshi K, Inoue K, Taniguchi M, Hashimoto H, Shintani N, Baba A et al (2007) A novel DISC1-interacting partner DISC1-binding zinc-finger protein: implication in the modulation of DISC1-dependent neurite outgrowth. *Mol Psychiatry* 12: 398–407
- Hattori T, Kaji M, Ishii H, Jureepon R, Takarada-Iemata M, Minh Ta H, Manh Le T, Konno A, Hirai H, Shiraishi Y et al (2017) CD38 positively regulates postnatal development of astrocytes cell-autonomously and oligodendrocytes non-cell-autonomously. *Glia* 65: 974–989
- Hayakawa K, Esposito E, Wang X, Terasaki Y, Liu Y, Xing C, Ji X, Lo EH (2016) Transfer of mitochondria from astrocytes to neurons after stroke. *Nature* 535: 551–555
- Hitti FL, Siegelbaum SA (2014) The hippocampal CA2 region is essential for social memory. *Nature* 508: 88–92
- Holt LM, Stoyanof ST, Olsen ML (2019) Magnetic cell sorting for in vivo and in vitro astrocyte, neuron, and microglia analysis. *Curr Protoc Neurosci* 88: e71
- Jin D, Liu HX, Hirai H, Torashima T, Nagai T, Lopatina O, Shnyder NA, Yamada K, Noda M, Seike T et al (2007) CD38 is critical for social behaviour by regulating oxytocin secretion. *Nature* 446: 41–45
- Kantzer CG, Boutin C, Herzig ID, Wittwer C, Reiss S, Tiveron MC, Drewes J, Rockel TD, Ohlig S, Ninkovic J et al (2017) Anti-ACSA-2 defines a novel monoclonal antibody for prospective isolation of living neonatal and adult astrocytes. *Glia* 65: 990–1004
- Kato I, Yamamoto Y, Fujimura M, Noguchi N, Takasawa S, Okamoto H (1999) CD38 disruption impairs glucose-induced increases in cyclic ADP-ribose, [Ca<sup>2+</sup>]<sub>i</sub>, and insulin secretion. *J Biol Chem* 274: 1869–1872
- Kay K, Sosa M, Chung JE, Karlsson MP, Larkin MC, Frank LM (2016) A hippocampal network for spatial coding during immobility and sleep. *Nature* 531: 185–190
- Kim S, Kim T, Lee HR, Jang EH, Ryu HH, Kang M, Rah SY, Yoo J, Lee B, Kim JI et al (2016) Impaired learning and memory in CD38 null mutant mice. *Mol Brain* 9: 16
- Kishi N, Macklis JD (2004) MECP2 is progressively expressed in post-migratory neurons and is involved in neuronal maturation rather than cell fate decisions. *Mol Cell Neurosci* 27: 306–321
- Clune CB, Jin B, DeNardo LA (2021) Linking mPFC circuit maturation to the developmental regulation of emotional memory and cognitive flexibility. *ELife* 10: e64567
- Koyama Y, Hattori T, Shimizu S, Taniguchi M, Yamada K, Takamura H, Kumamoto N, Matsuzaki S, Ito A, Katayama T et al (2013) DBZ (DISC1-binding zinc finger protein)-deficient mice display abnormalities in basket cells in the somatosensory cortices. *J Chem Neuroanat* 53: 1–10
- Lee HC (2001) Physiological functions of cyclic ADP-ribose and NAADP as calcium messengers. *Annu Rev Pharmacol Toxicol* 41: 317–345
- Lizen B, Claus M, Jeannotte L, Rijli FM, Gofflot F (2015) Perinatal induction of Cre recombination with tamoxifen. *Transgenic Res* 24: 1065–1077
- Lopez-Hidalgo M, Schummers J (2014) Cortical maps: a role for astrocytes? *Curr Opin Neurobiol* 24: 176–189
- Malavasi F, Deaglio S, Funaro A, Ferrero E, Horenstein AL, Ortolan E, Vaisitti T, Aydin S (2008) Evolution and function of the ADP ribosyl cyclase/CD38 gene family in physiology and pathology. *Physiol Rev* 88: 841–886
- Martucci LL, Amar M, Chausseot R, Benet G, Bauer O, de Zelicourt A, Nosjean A, Launay JM, Callebert J, Sebrie C et al (2019) A multiscale analysis in CD38(–/–) mice unveils major prefrontal cortex dysfunctions. *FASEB J* 33: 5823–5835
- Mori T, Tanaka K, Buffo A, Wurst W, Kuhn R, Gotz M (2006) Inducible gene deletion in astroglia and radial glia—a valuable tool for functional and lineage analysis. *Glia* 54: 21–34
- Nagai J, Rajbhandari AK, Gangwani MR, Hachisuka A, Coppola G, Masmanidis SC, Fanselow MS, Khakh BS (2019) Hyperactivity with disrupted attention by activation of an astrocyte synaptogenic cue. *Cell* 177: 1280–1292
- Nelissen TP, Bamford RA, Tochtiani S, Akkus K, Kudzinskas A, Yokoi K, Okamoto H, Yamamoto Y, Burbach JPH, Matsuzaki H et al (2018) CD38 is required for dendritic organization in visual cortex and hippocampus. *Neuroscience* 372: 114–125
- Ohlig S, Clavreul S, Thorwirth M, Simon-Ebert T, Bocchi R, Ulbricht S, Kannayian N, Rossner M, Sirko S, Smialowski P et al (2021) Molecular diversity of diencephalic astrocytes reveals adult astrogenesis regulated by Smad4. *EMBO J* 40: e107532
- Okamoto H, Takasawa S (2021) Okamoto model for necrosis and its expansions, CD38-cyclic ADP-ribose signal system for intracellular Ca(2+) mobilization and Reg (regenerating gene protein)-Reg receptor system for cell regeneration. *Proc Jpn Acad Ser B Phys Biol Sci* 97: 423–461
- Okuyama T, Kitamura T, Roy DS, Itoharu S, Tonegawa S (2016) Ventral CA1 neurons store social memory. *Science* 353: 1536–1541
- Oliva A, Fernandez-Ruiz A, Leroy F, Siegelbaum SA (2020) Hippocampal CA2 sharp-wave ripples reactivate and promote social memory. *Nature* 587: 264–269
- Orr AG, Hsiao EC, Wang MM, Ho K, Kim DH, Wang X, Guo W, Kang J, Yu GQ, Adame A et al (2015) Astrocytic adenosine receptor A2A and Gs-coupled signaling regulate memory. *Nat Neurosci* 18: 423–434
- Park H, Poo MM (2013) Neurotrophin regulation of neural circuit development and function. *Nat Rev Neurosci* 14: 7–23
- Pellow S, Chopin P, File SE, Briley M (1985) Validation of open/closed arm entries in an elevated plus-maze as a measure of anxiety in the rat. *J Neurosci Methods* 14: 149–167
- Risher WC, Patel S, Kim IH, Uezu A, Bhagat S, Wilton DK, Pilaz LJ, Singh Alvarado J, Calhan OY, Silver DL et al (2014) Astrocytes refine cortical connectivity at dendritic spines. *eLife* 3: e04047
- Sala M, Braida D, Donzelli A, Martucci R, Busnelli M, Bulgheroni E, Rubino T, Parolaro D, Nishimori K, Chini B (2013) Mice heterozygous for the oxytocin receptor gene (Oxtr(+/-)) show impaired social behaviour but not increased aggression or cognitive inflexibility: evidence of a selective haploinsufficiency gene effect. *J Neuroendocrinol* 25: 107–118
- Samaco RC, McGraw CM, Ward CS, Sun Y, Neul JL, Zoghbi HY (2013) Female Mecp2(+/-) mice display robust behavioral deficits on two different genetic backgrounds providing a framework for pre-clinical studies. *Hum Mol Genet* 22: 96–109
- Shinohara M, Arakawa H, Oda Y, Shiraki N, Sugiura S, Nishiuchi T, Satoh T, Iino K, Leo S, Kato Y et al (2021) Coculture with hiPS-derived intestinal cells enhanced human hepatocyte functions in a pneumatic-pressure-driven two-organ microphysiological system. *Sci Rep* 11: 5437
- Singh SK, Stogsdill JA, Pulimood NS, Dingsdale H, Kim YH, Pilaz LJ, Kim IH, Manhaes AC, Rodrigues WS Jr, Pamukcu A et al (2016) Astrocytes assemble Thalamocortical synapses by bridging NRX1alpha and NL1 via Hevin. *Cell* 164: 183–196
- Smrt RD, Eaves-Egenes J, Barkho BZ, Santistevan NJ, Zhao C, Aimone JB, Gage FH, Zhao X (2007) Mecp2 deficiency leads to delayed maturation and altered gene expression in hippocampal neurons. *Neurobiol Dis* 27: 77–89
- Sun Q, Li X, Li A, Zhang J, Ding Z, Gong H, Luo Q (2020) Ventral hippocampal-prefrontal interaction affects social behavior via Parvalbumin positive neurons in the medial prefrontal cortex. *iScience* 23: 100894

- Takarada-Iemata M, Kezuka D, Takeichi T, Ikawa M, Hattori T, Kitao Y, Hori O (2014) Deletion of N-myc downstream-regulated gene 2 attenuates reactive astrogliosis and inflammatory response in a mouse model of cortical stab injury. *J Neurochem* 130: 374–387
- Trapnell C, Hendrickson DG, Sauvageau M, Goff L, Rinn JL, Pachter L (2013) Differential analysis of gene regulation at transcript resolution with RNA-seq. *Nat Biotechnol* 31: 46–53
- Tzakis N, Holahan MR (2019) Social memory and the role of the hippocampal CA2 region. *Front Behav Neurosci* 13: 233
- Xing B, Mack NR, Guo KM, Zhang YX, Ramirez B, Yang SS, Lin L, Wang DV, Li YC, Gao WJ (2021) A subpopulation of prefrontal cortical neurons is required for social memory. *Biol Psychiatry* 89: 521–531
- Zhang JB, Chen L, Lv ZM, Niu XY, Shao CC, Zhang C, Pruski M, Huang Y, Qi CC, Song NN et al (2016) Oxytocin is implicated in social memory deficits induced by early sensory deprivation in mice. *Mol Brain* 9: 98
- Zhang N, Zhang Z, He R, Li H, Ding S (2020) GLAST-CreER(T2) mediated deletion of GDNF increases brain damage and exacerbates long-term stroke outcomes after focal ischemic stroke in mouse model. *Glia* 68: 2395–2414



## Expanded View Figures

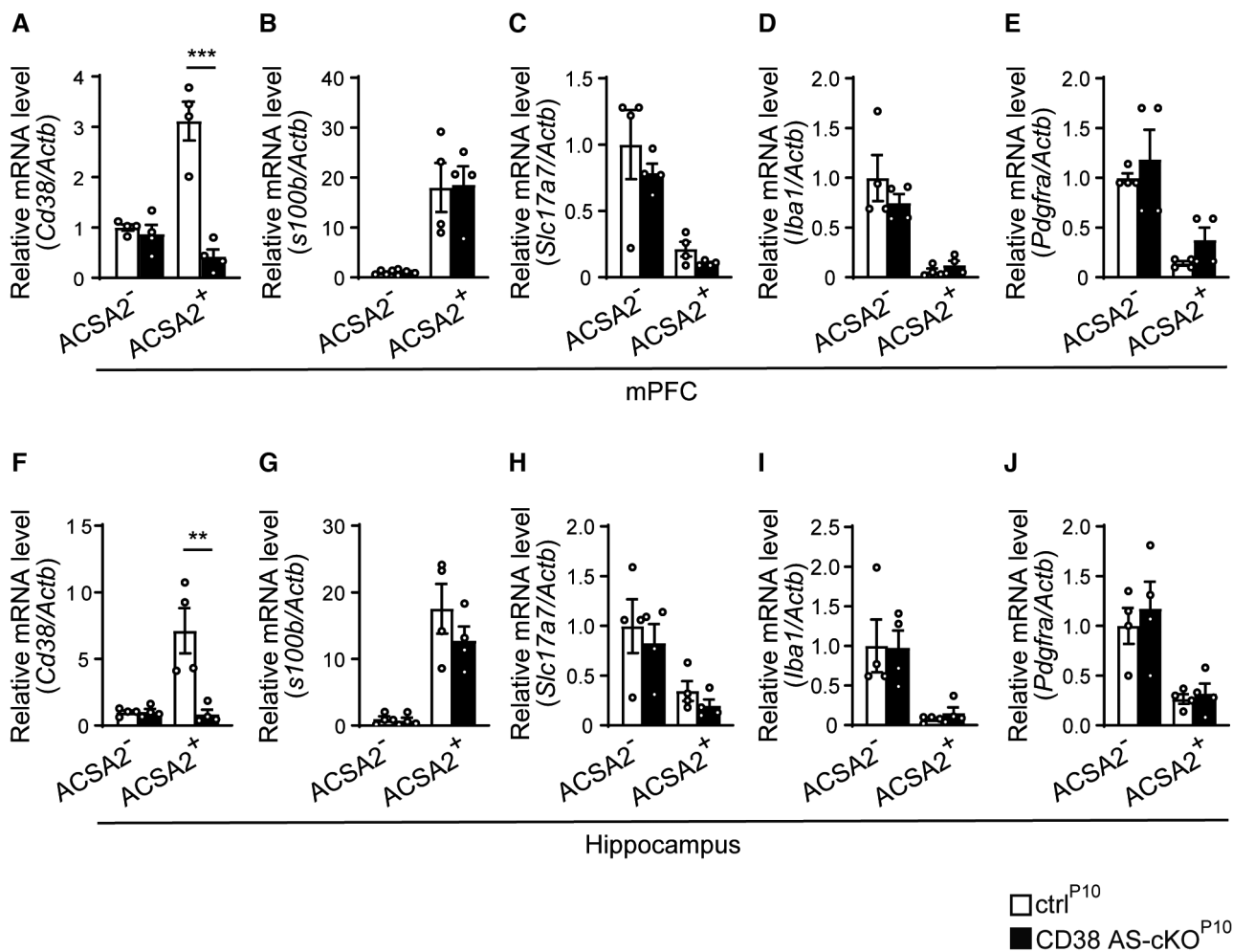


**Figure EV1. CD38 is specifically deleted in astrocytes of CD38 AS-cKO<sup>P10</sup> mice.**

A–J RT-qPCR analysis of *Cd38*, *S100b*, *Slc17a7* (VGLUT1), *Iba1*, *Pdgfra* mRNA in ACSA2 negative or positive fraction from the mPFC (A–E) and hippocampus (F–J) of ctrl<sup>P10</sup> and CD38 AS-cKO<sup>P10</sup> mice. Astrocytes were enriched by magnetic bead assisted cell sorting (MACS) for astrocytes-specific ACSA2 antigen ( $n = 4$  animals per genotype, two-way ANOVA followed by Bonferroni's multiple comparisons test).

Data information: Data represent means  $\pm$  SEM, \*\* $P < 0.01$ , \*\*\* $P < 0.001$ .

**Figure EV2. Astrocyte-specific deletion of CD38 decreases expression of GFAP, s100 $\beta$  and Cx43 in the developing mPFC.**

- A Representative western blots of CD38, GFAP, Cx43, NDRG2, VGlut1, PSD95, MAG, and  $\beta$ -actin in the mPFC of ctrl<sup>P10</sup> and CD38 AS-cKO<sup>P10</sup> mice at P21 (two animals per genotype are shown).
- B–H Relative optical densities of CD38, GFAP, Cx43, NDRG2, VGlut1, PSD95, MAG, and  $\beta$ -actin normalized to the loading control  $\beta$ -actin ( $n = 4$  animals per genotype, two-tailed unpaired Student's  $t$ -test).
- I Representative western blots of CD38 and  $\beta$ -actin in the mPFC of ctrl<sup>P42</sup> and CD38 AS-cKO<sup>P42</sup> mice at P84 (two animals per genotype are shown).
- J Bar graphs depict the relative optical density of CD38 and  $\beta$ -actin normalized to the loading control  $\beta$ -actin ( $n = 3$  animals per genotype, two-tailed unpaired Student's  $t$ -test).
- K–T (K, M, O, Q, S) Immunohistochemistry for GFAP, s100 $\beta$ , NDRG2 and SOX9 in the mPFC and MBP in the motor cortex of ctrl<sup>P10</sup> and CD38 AS-cKO<sup>P10</sup> mice at P21. Nuclei were counterstained with DAPI. Scale bars, 50  $\mu$ m (K, M, O, and Q), and 100  $\mu$ m (S). (L, N, P, R, T) Quantification of astrocyte-specific protein-positive cells and MBP intensity ( $n = 4$  animals per genotype, two-tailed unpaired Student's  $t$ -test).

Data information: Data represent means  $\pm$  SEM. \* $P < 0.05$ , \*\* $P < 0.01$ , \*\*\* $P < 0.001$ .

Source data are available online for this figure.

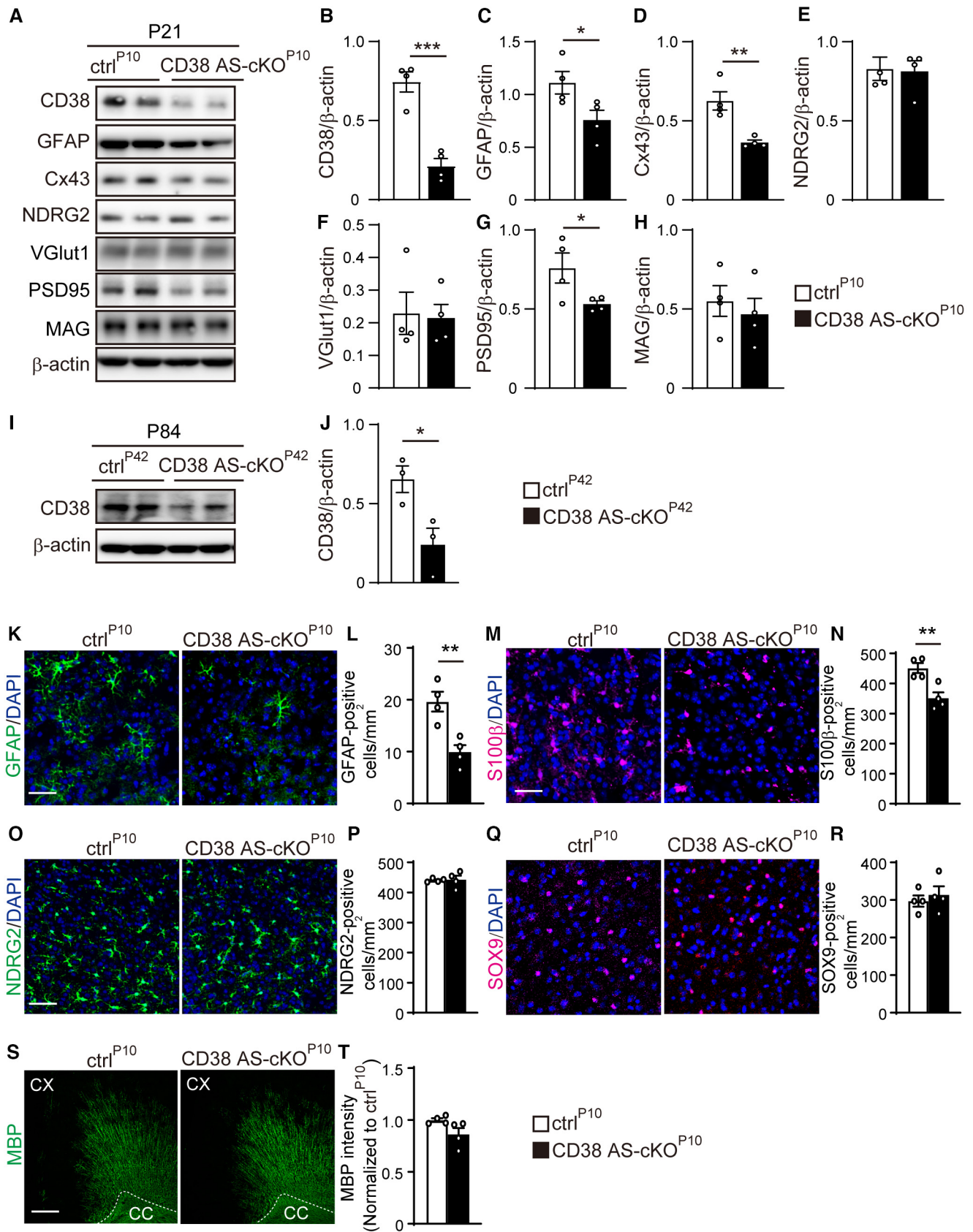
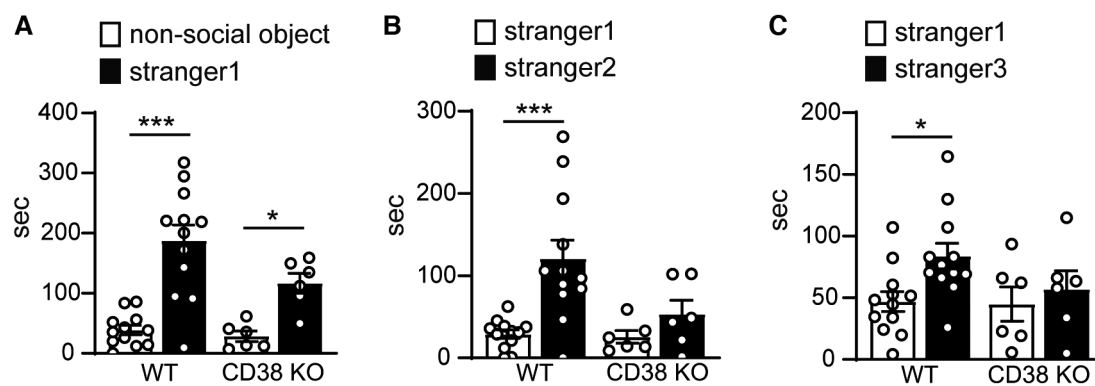


Figure EV2.



**Figure EV3. Social novelty is impaired in constitutive CD38 KO mice.**

- A Sociability of WT and CD38 KO mice ( $n = 6$  and  $12$  animals in WT and CD38 KO mice, respectively, two-way ANOVA followed by Bonferroni's multiple comparisons test).
- B Social novelty of WT and CD38 KO mice ( $n = 6$  and  $12$  animals in WT and CD38 KO mice, respectively, two-way ANOVA followed by Bonferroni's multiple comparisons test).
- C Social memory of WT and CD38 KO mice ( $n = 6$  and  $12$  animals in WT and CD38 KO mice, respectively, two-way ANOVA followed by Bonferroni's multiple comparisons test).

Data information: Data represent means  $\pm$  SEM. \* $P < 0.05$ , \*\*\* $P < 0.001$ .

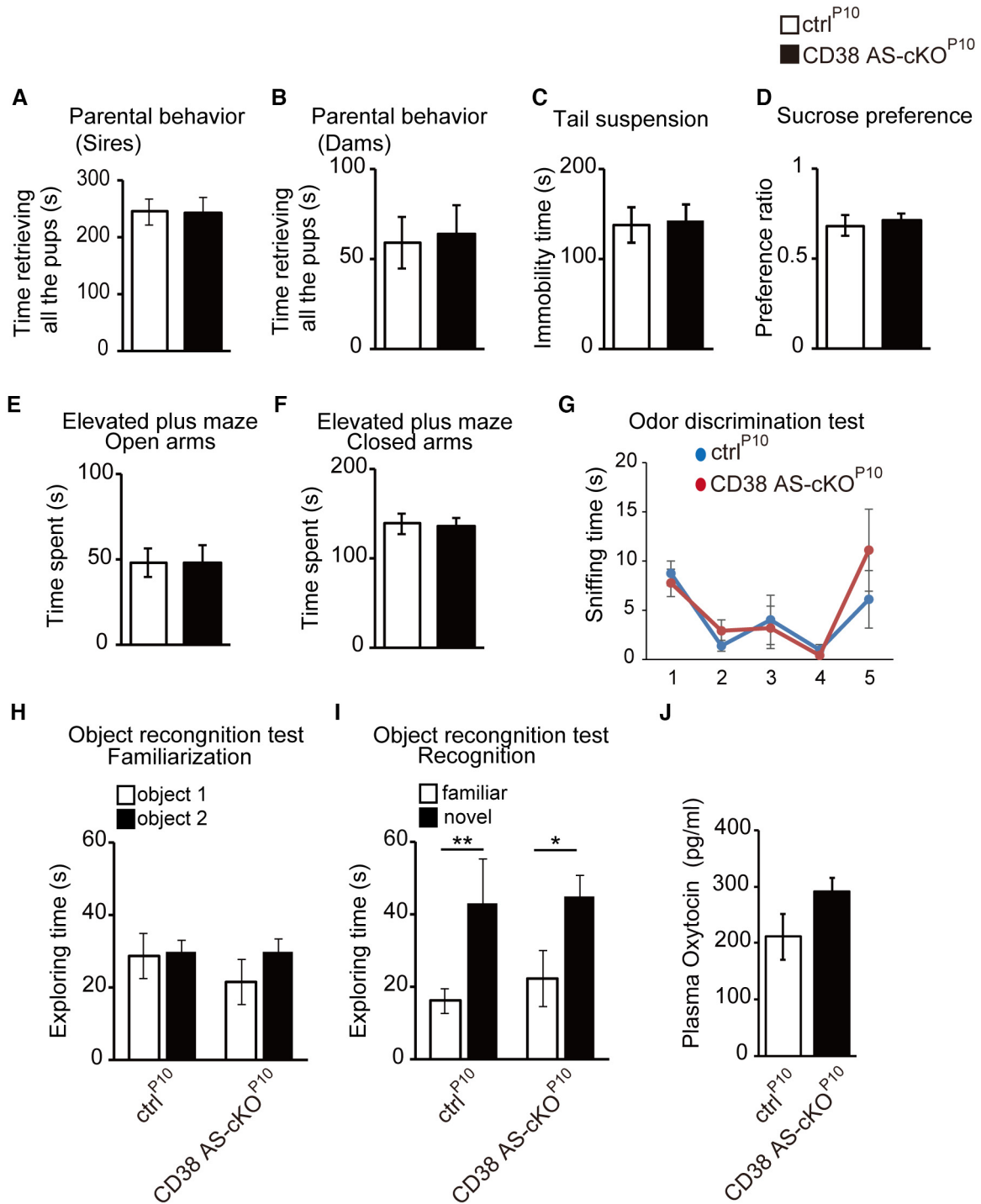


Figure EV4.



**Figure EV4. Behavioral phenotypes except social memory are not impaired in CD38 AS-cKO<sup>P10</sup> mice.**

- A, B Pup retrieval behavior. Time to complete retrieving all the pups of ctrl<sup>P10</sup> and CD38 AS-cKO<sup>P10</sup> sires (A) and dams (B) ( $n = 5$  animals per genotype, two-tailed unpaired Student's  $t$ -test).
- C Tail suspension test of ctrl<sup>P10</sup> and CD38 AS-cKO<sup>P10</sup> mice ( $n = 10$  animals per genotype, two-tailed unpaired Student's  $t$ -test).
- D Sucrose preference test of ctrl<sup>P10</sup> and CD38 AS-cKO<sup>P10</sup> mice ( $n = 10$  animals per genotype, two-tailed unpaired Student's  $t$ -test).
- E, F Elevated plus maze test. Time in open arms (E) and closed arms (F) for ctrl<sup>P10</sup> and CD38 AS-cKO<sup>P10</sup> mice ( $n = 10$  animals per genotype, two-tailed unpaired Student's  $t$ -test).
- G Odor discrimination test of ctrl<sup>P10</sup> and CD38 AS-cKO<sup>P10</sup> mice ( $n = 5$  animals per genotype, two-way ANOVA followed by Bonferroni's multiple comparisons test).
- H, I Object recognition test of ctrl<sup>P10</sup> and CD38 AS-cKO<sup>P10</sup> mice. Exploring time during the acquisition phase (H) and the recognition trial (I) ( $n = 6$  animals per genotype, two-way ANOVA followed by Bonferroni's multiple comparisons test).
- J Plasma oxytocin concentrations in ctrl<sup>P10</sup> and CD38 AS-cKO<sup>P10</sup> mice ( $n = 7$  and  $10$  animals in ctrl<sup>P10</sup> and CD38 AS-cKO<sup>P10</sup> mice, respectively; two-tailed unpaired Student's  $t$ -test).

Data information: Data represent means  $\pm$  SEM. \* $P < 0.05$ , \*\* $P < 0.01$ .

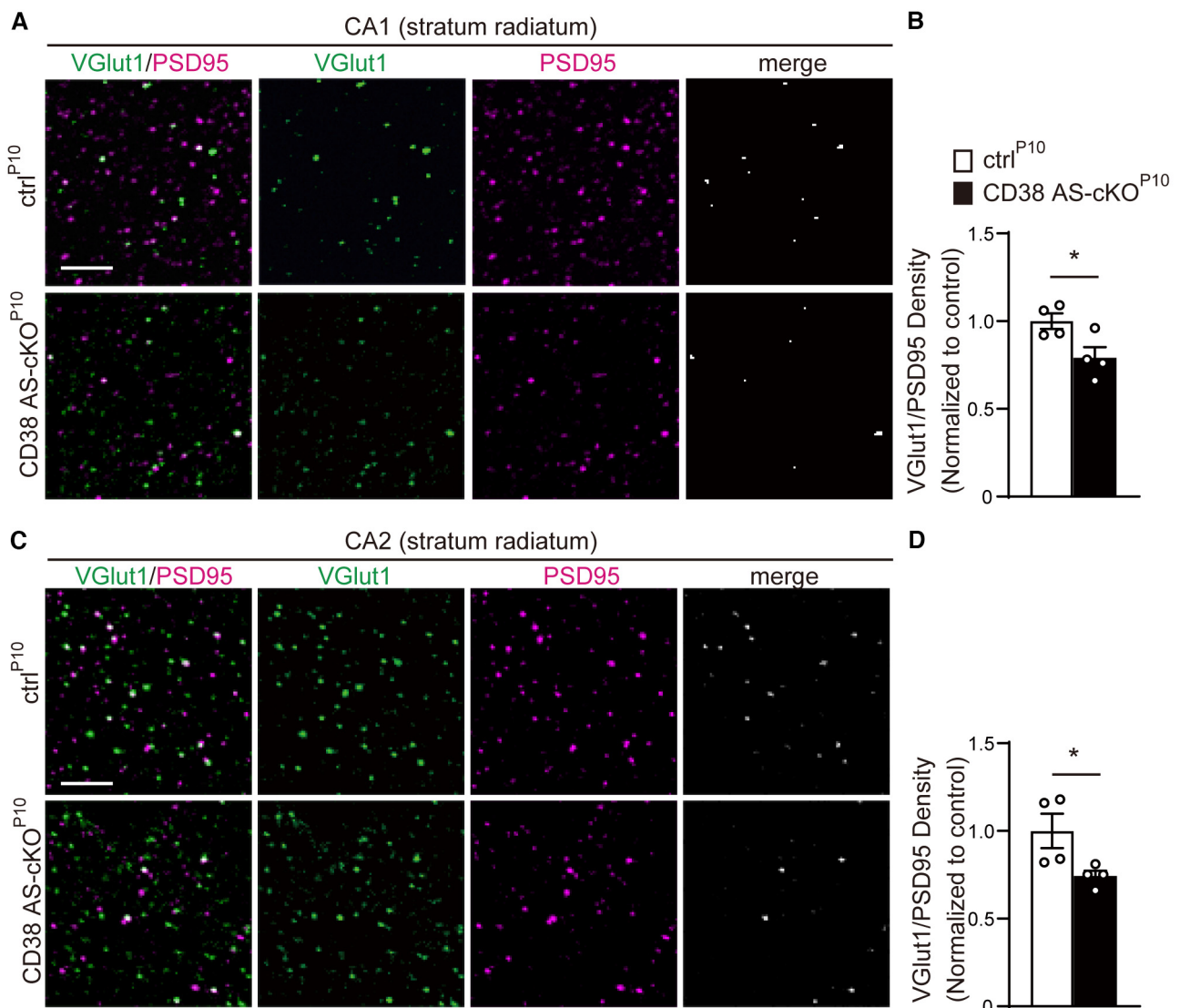


Figure EV5.

**Figure EV5. Excitatory synapses are reduced in the hippocampal neurons in CD38 AS-cKO<sup>P10</sup> mice.**

A–D (A, C) Immunohistochemistry for VGLut1 (green) and PSD95 (magenta) in the stratum radiatum of the CA1 (A) and CA2 (C) of ctrl<sup>P10</sup> and CD38 AS-cKO<sup>P10</sup> mice at P70. The VGLut1 and PSD95 channels are separated in the middle panels. Right panels are colocalized VGLut1 and PSD95 puncta. Scale bar, 10  $\mu$ m. (B, D) Quantification synapses (colocalization of VGLut1 and PSD95) in each area of the hippocampus ( $n = 4$  animals per genotype, two-tailed unpaired Student's  $t$ -test).

Data information: Data represent means  $\pm$  SEM. \* $P < 0.05$ .

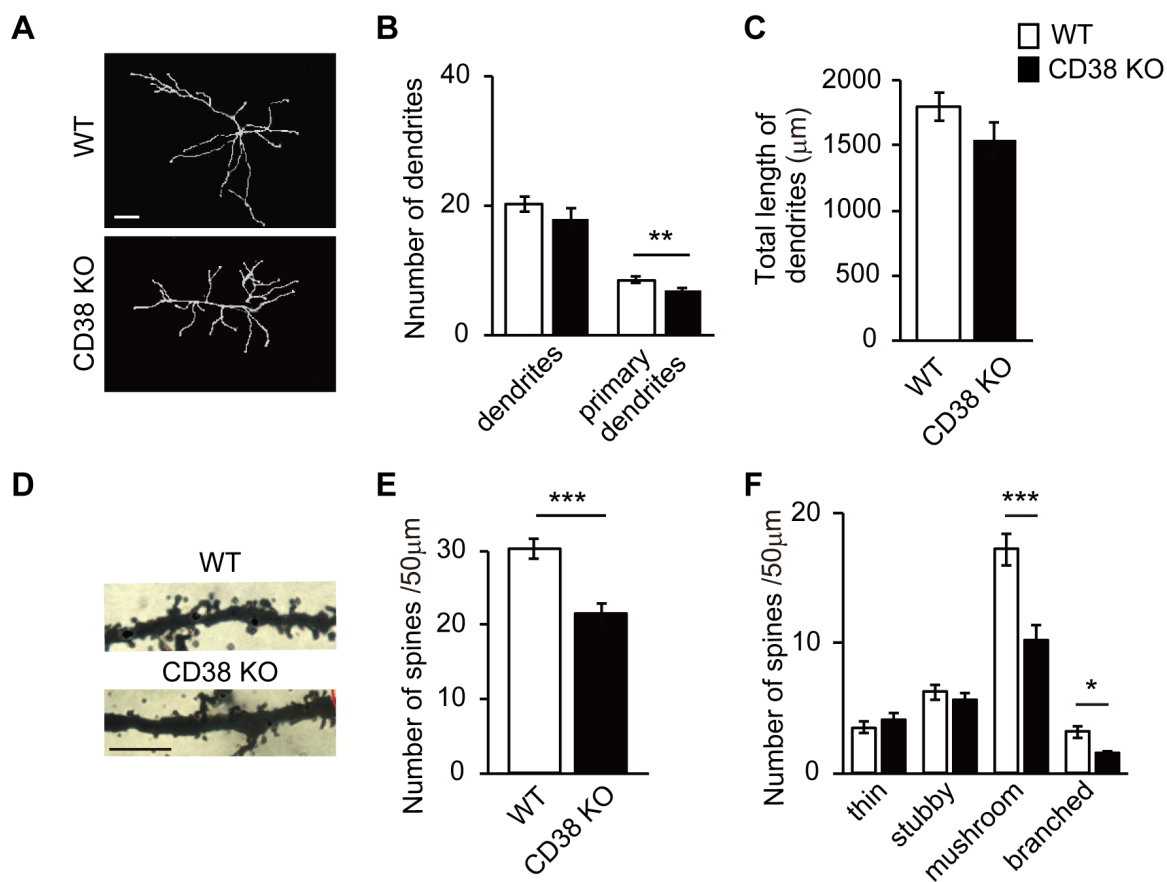
# Appendix

## Postnatal expression of CD38 in astrocytes regulates synapse formation and adult social memory

Tsuyoshi Hattori<sup>1\*</sup>, Stanislav M Cherepanov<sup>2</sup>, Ryo Sakaga<sup>1</sup>, Jureepon Roboon<sup>1</sup>, Dinh Thi Nguyen<sup>1</sup>, Hiroshi Ishii<sup>1</sup>, Mika Takarada-Iemata<sup>1</sup>, Takumi Nishiuchi<sup>3</sup>, Takayuki Kannon<sup>4</sup>, Kazuyoshi Hosomichi<sup>4</sup>, Atsushi Tajima<sup>4</sup>, Yasuhiko Yamamoto<sup>5</sup>, Hiroshi Okamoto<sup>5,6</sup>, Akira Sugawara<sup>7</sup>, Haruhiro Higashida<sup>2</sup>, Osamu Hori<sup>1</sup>

### Table of contents

Appendix Figure S1.	Page 2-3
Appendix Figure S2.	Page 4
Appendix Figure S3.	Page 5
Appendix Figure S4.	Page 6
Appendix Figure S5.	Page 7
Appendix Figure S6.	Page 8



**Appendix Figure S1. Morphology of dendrites and spines is altered in the mPFC pyramidal neurons in constitutive CD38 KO mice.**

(A) Images of tracing of Golgi-stained pyramidal neurons in the mPFC of WT and CD38 KO mice. Scale bar, 20  $\mu\text{m}$ .

(B, C) Quantification of the total number (B) or total length (C) of dendrites and primary dendrites in WT and CD38 KO mice. ( $n = 24$  cells from four animals per genotype, two-way ANOVA followed by Bonferroni's multiple comparisons test).

(D) Images of Golgi-stained pyramidal neurons in the mPFC of WT and CD38 KO mice. Scale bar, 5  $\mu\text{m}$ .

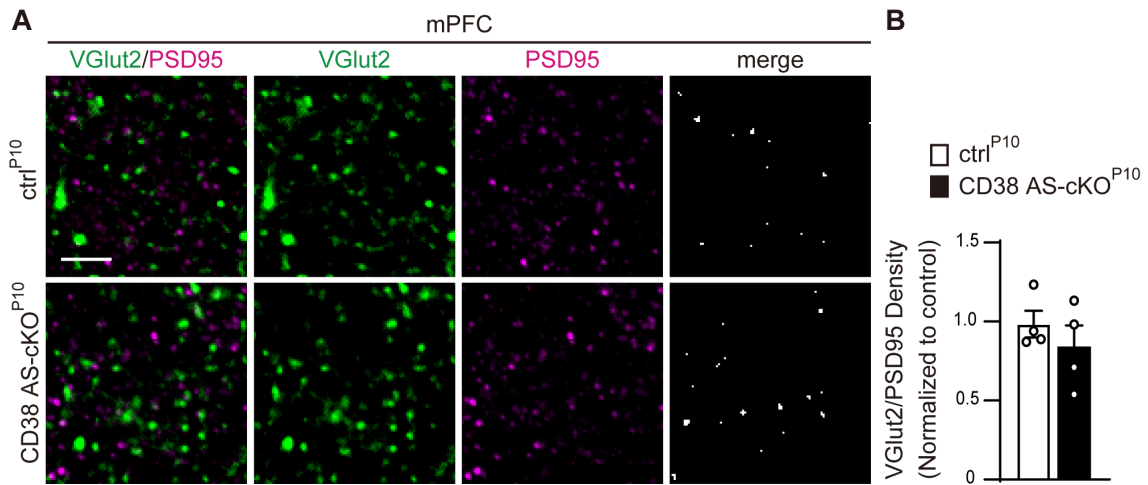
(E) Quantification of the total number of spines on apical dendrites of WT and CD38 KO mice. ( $n = 16$  dendrites from four animals per genotype, Student's unpaired  $t$ -test).

(F) The percentage of branched, mushroom, stubby and thin-type spines in cortical apical dendritic spines. ( $n = 16$  dendrites from four animals per genotype, two-way ANOVA followed by

Bonferroni's multiple comparisons test).

Data information: \* $p < 0.05$ , \*\* $p < 0.01$ , \*\*\* $p < 0.001$  vs WT. Data represent means  $\pm$  SEM.



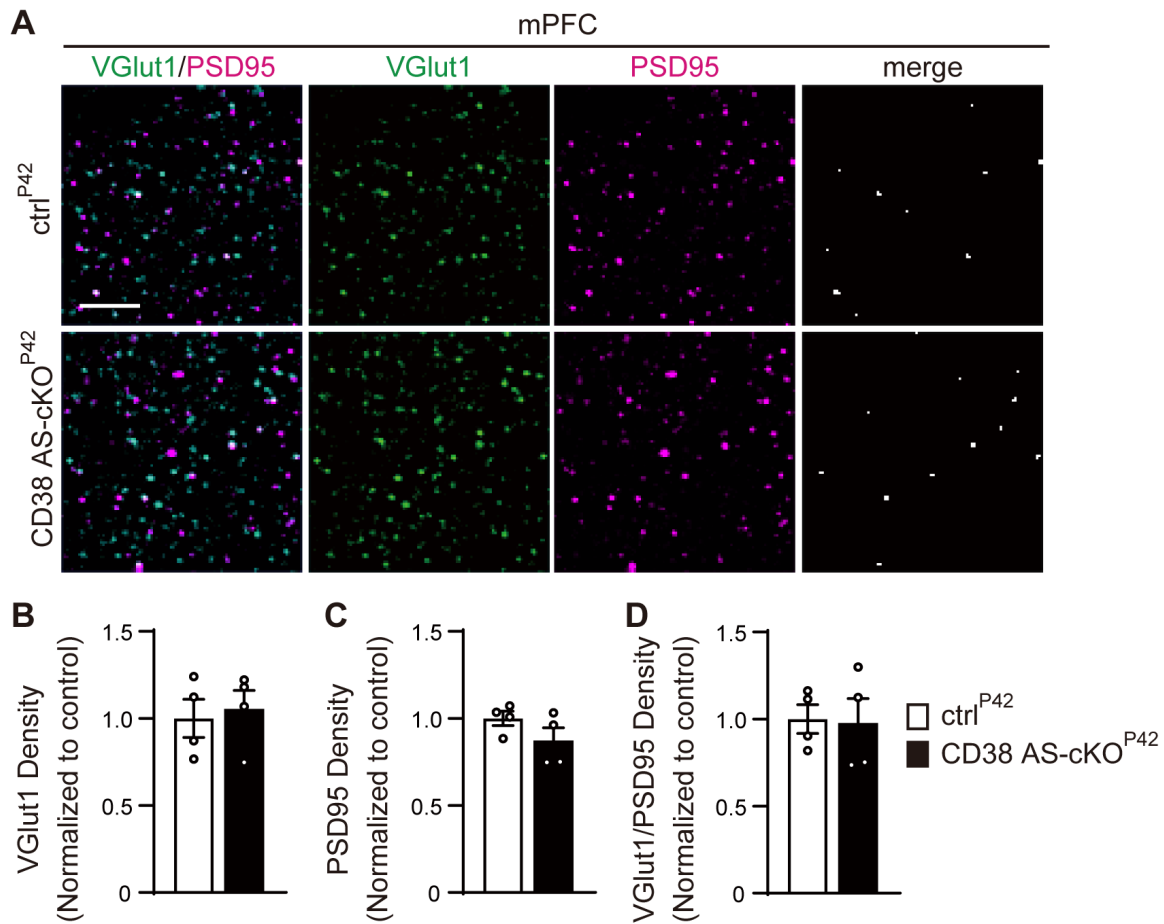


**Appendix Figure S2. Number of VGlut2+ excitatory synapses are not changed in the mPFC of CD38 AS-cKO<sup>P10</sup> mice.**

(A) Immunohistochemistry for VGlut2 (green) and PSD95 (magenta) in the mPFC of ctrl<sup>P10</sup> and CD38 AS-cKO<sup>P10</sup> mice at P70. The VGlut2 and PSD95 channels are separated in the middle panels. Right panels are colocalized VGlut2 and PSD95 puncta. Scale bar, 10  $\mu$ m.

(B) Quantification of VGlut2+ synapse densities in the mPFC in ctrl<sup>P10</sup> and CD38 AS-cKO<sup>P10</sup> mice. ( $n = 4$  animals per genotype, Student's unpaired  $t$ -test).

Data information: Data represent means  $\pm$  SEM.

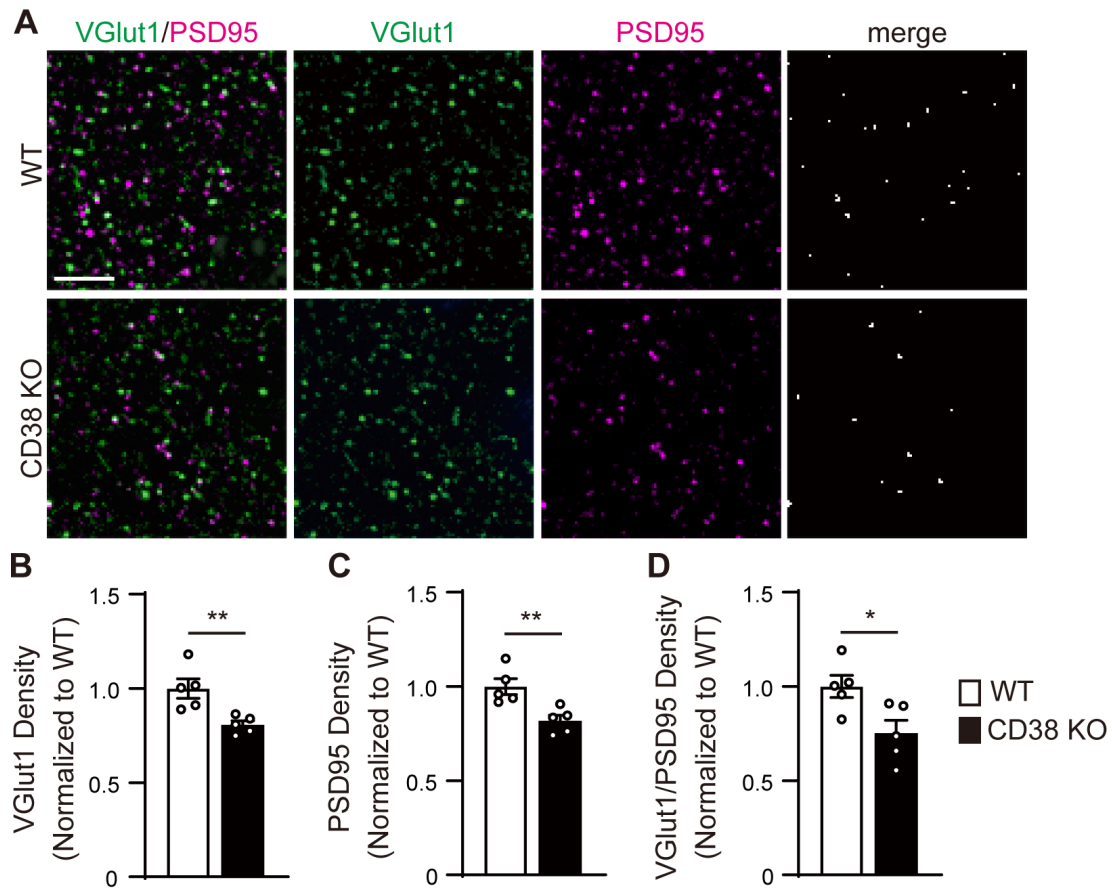


**Appendix Figure S3. Number of excitatory synapses are not changed in the mPFC cortical pyramidal neurons in CD38 AS-cKO<sup>P42</sup> mice.**

(A) Immunohistochemistry for VGlut1 (green) and PSD95 (magenta) in the mPFC of ctrl<sup>P42</sup> and CD38 AS-cKO<sup>P42</sup> mice at P70. The VGlut1 and PSD95 channels are separated in the middle panels. Right panels are colocalized VGlut1 and PSD95 puncta. Scale bar, 10  $\mu$ m.

(B–D) Quantification of VGlut1, PSD95 and synapse densities in the mPFC in ctrl<sup>P42</sup> and CD38 AS-cKO<sup>P42</sup> mice. ( $n = 4$  animals per genotype, Student's unpaired  $t$ -test).

Data information: Data represent means  $\pm$  SEM.

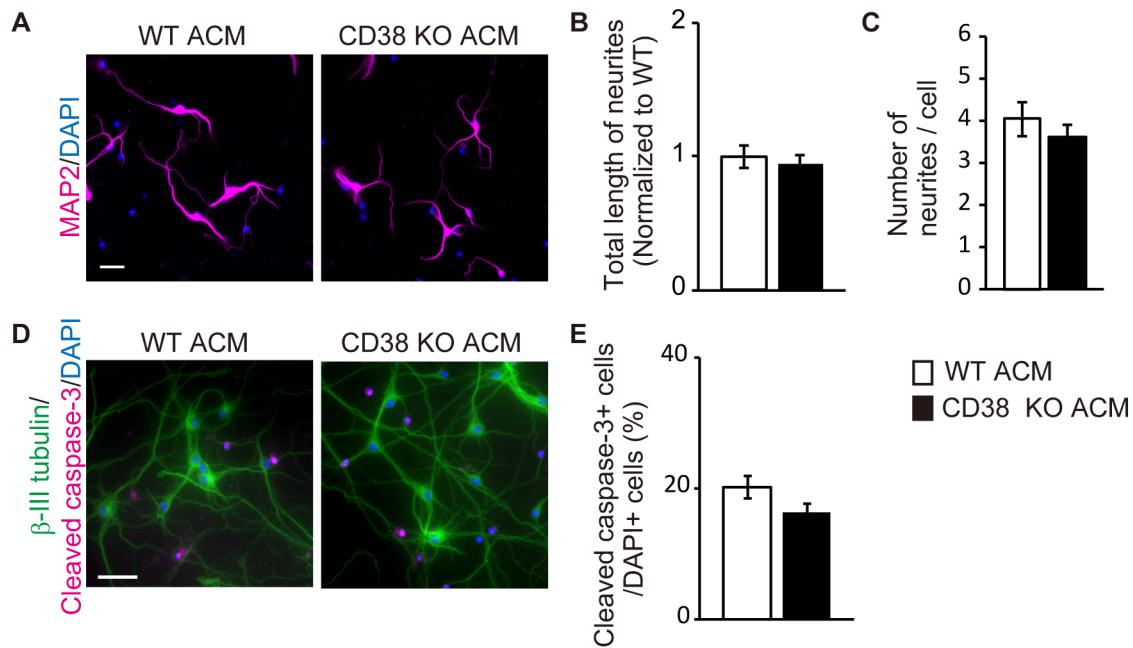


**Appendix Figure S4. Excitatory synapses are reduced in the mPFC cortical pyramidal neurons in constitutive CD38 KO mice.**

(A) Immunohistochemistry for VGLut1 (green) and PSD95 (magenta) in the mPFC of WT and CD38 KO mice at P70. The VGLut1 and PSD95 channels are separated in the middle panels. Right panels are colocalized VGLut1 and PSD95 puncta. Scale bar, 10  $\mu$ m.

(B–D) Quantification of VGLut1, PSD95 and synapse densities in the mPFC in WT and CD38 KO mice. ( $n = 5$  animals per genotype, Student’s unpaired  $t$ -test).

Data information: \*  $p < 0.05$ , \*\*  $p < 0.01$ . Data represent means  $\pm$  SEM.



**Appendix Figure S5. CD38 KO ACM does not affect neurite outgrowth and cell viability of cortical neurons.**

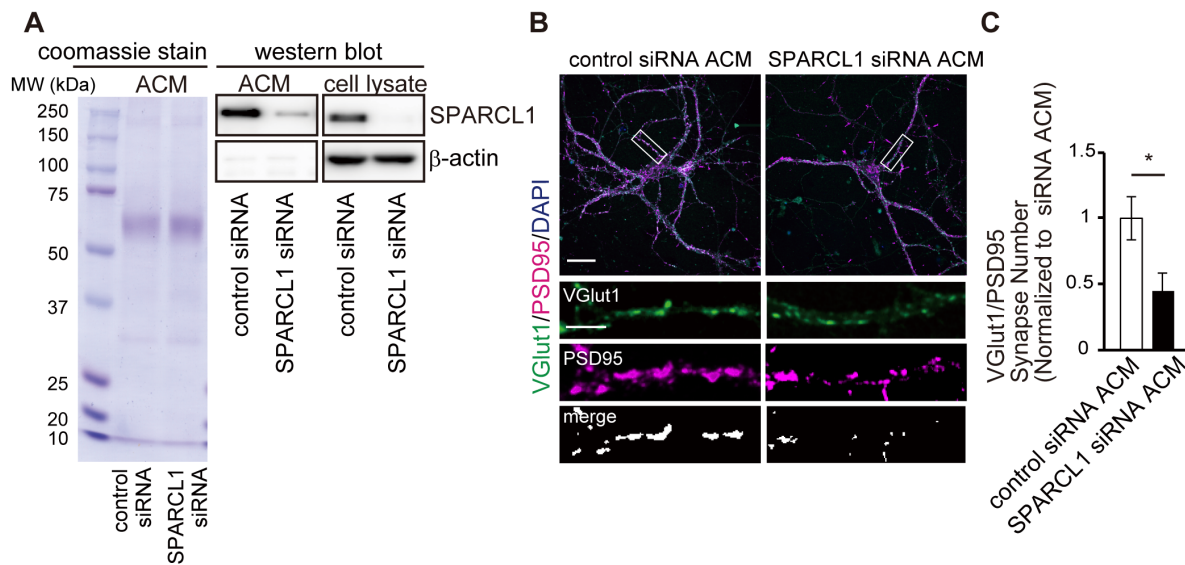
(A) Representative images of cortical neurons cultured in ACM of WT or CD38 KO mice at 6 DIV. Cells were stained with antibody against MAP2 (magenta). Nuclei were counterstained with DAPI. Scale bar, 50  $\mu$ m.

(B, C) Quantification of the total length of neurites and number of neurites per cell. ( $n = 40$  cells per genotype from three independent culture, Student's unpaired  $t$ -test).

(D) Representative images of cortical neurons cultured in ACM of WT or CD38 KO mice at 6 DIV. Cells are stained with antibody against  $\beta$ -III tubulin (green) and Cleaved caspase-3 (magenta). Nuclei were counterstained with DAPI. Scale bar, 50  $\mu$ m.

(E) Quantification of cleaved caspase-3 positive cells out of DAPI positive cells. ( $n = 40$ , Student's unpaired  $t$ -test).

Data information: Data represent means  $\pm$  SEM.



**Appendix Figure S6. ACM of SPARCL1-knockdown astrocytes reduces synapse formation of cortical neurons.**

(A) Coomassie stain shows the total protein composition of ACM of control siRNA or SPARCL1 siRNA-transfected astrocytes. Representative western blot images of SPARCL1 and  $\beta$ -actin in ACM and cell lysate of astrocytes transfected with control or SPARCL1 siRNA.

(B) Representative images of cortical neurons cultured for 14 DIV in ACM of control or SPARCL1 siRNA-transfected astrocytes. Insets show individual channels for VGlut1 (green) and PSD95 (magenta) staining, as well as the merged image. Nuclei were counterstained with DAPI. Scale bar, 20  $\mu$ m (main image) and 10  $\mu$ m (inset).

(C) Quantification of synapse number in cortical neurons cultured in ACM of control or SPARCL1 siRNA-transfected astrocytes. ( $n = 20$  cells per condition from three independent culture, Student's unpaired  $t$ -test).

Data information: \*  $p < 0.05$ . Data represent means  $\pm$  SEM.